RESEARCH MEMORANDUM

EXPERIMENTAL AND THEORETICAL STUDY OF FACTORS INFLUENCING THE LONGITUDINAL STABILITY OF AN AIR-TO-AIR MISSILE AT A MACH NUMBER OF 1.4

By S. Sherman Edwards

Ames Aeronautical Laboratory
Moffett Field, Calif.

NATIONAL ADVISORY COMMITTEE
FOR AERONAUTICS

WASHINGTON

January 21, 1952

NATIONAL ADVISORY COMMITTEE FOR AERONAUTICS

RESEARCH MEMORANDUM

EXPERIMENTAL AND THEORETICAL STUDY OF FACTORS INFLUENCING THE LONGITUDINAL STABILITY OF AN AIR-TO-AIR MISSILE AT A MACH NUMBER OF 1.4

By S. Sherman Edwards

SUMMARY

Approximate methods of analysis are applied to the estimation of the normal force and pitching moment of the body and the wing-body and tail-body combinations of an air-to-air missile and to the estimation of the same characteristics of the complete configuration. The results of the calculations are compared with experimentally determined normal force and pitching moments for the missile model obtained at a Mach number of 1.4, at a Reynolds number of 1.26 million, based on the mean aerodynamic chord of the wing. The experimental data and the results of the calculations are presented for a range of angle of attack up to 22°, for angles of bank between 0° and 45° in 11.25° increments.

The comparison between calculated results and the experimental data shows that, for the missile investigated, the longitudinal stability and normal-force characteristics can be accurately estimated. The methods used are discussed in detail.

INTRODUCTION

The aerodynamic design of air-to-air missiles is primarily a study of aerodynamic interference effects. The properties of such missiles are no longer to a first order the sum of the aerodynamic characteristics of the isolated wing and the isolated body plus small interference effects as is the usual case for airplanes. Because of limitations often placed on the span of the lifting surfaces, the wing span may be less than twice the body diameter; and the resulting mutual interaction of the flow fields of the wing and body results in interference forces and moments of the same order of magnitude as those for the isolated elements.

A further problem exists in the interference of tandem wing arrangements. This problem has been present in airplane design but has become more difficult for missiles because the span of the rear wing in some cases is nearly equal to or larger than that of the forward wing. The forces induced on the rear wing of a tandem arrangement and the moments thereby provided have therefore become correspondingly more significant. In addition, the necessity of attaining large lateral accelerations in target-seeking maneuvers has led to the use of cruciform wings with attendant complex wing-wing interference.

Recognition of this problem has led to many extensive theoretical investigations of interference problems which, because of the difficult nature of the analysis, involve certain simplifying approximations (references 1 to 5). In all cases, the theoretical solutions are restricted to inviscid flow about wings and bodies at small incidence. In some cases, a further limitation stipulating that the wing and body combination is very slender is imposed on the theoretical results, thereby restricting their usefulness.

A number of experimental investigations of missile interference problems have been made to assess the accuracy of the theoretical studies. (See for instance references 6 and 7.) The results of these investigations have shown in some cases that theory and experiment do not correspond primarily because the limitations of the theory have been exceeded, particularly in those cases involving viscous effects and those concerned with large wing incidences which are of great concern in missile design. The present investigation was undertaken for the purpose of extending the comparison between theory and experiment to large angles of attack and to provide additional information and methods of analysis for use in missile design. The present investigation is concerned solely with the lift and with the longitudinal stability of one particular missile configuration.

SYMBOLS

a	body radius, feet
B	body
$\bar{c}$	mean aerodynamic chord of the exposed area of the wing, feet
C_m	pitching-moment coefficient about the model center of gravity (based upon the exposed area of two wing panels and $\bar{c}$) $\left(\frac{\text{pitching moment}}{qS_W\bar{c}} \right)$

C_N normal-force coefficient (based upon the exposed area of two wing panels) $\left(\frac{\text{normal force}}{qS_W}\right)$

$c_{N_{\alpha_W}}$ normal-force curve slope for isolated wing determined from slender wing theory $\left(\frac{\partial c_N}{\partial \alpha}\right)_W$

$c_{N_{\alpha_{W+B}}}$ normal-force curve slope for wing in combination with cylindrical body determined from slender wing-body theory $\left(\frac{\partial c_N}{\partial \alpha}\right)_{W+B}$

$C_{N_{\alpha_W}}$ normal-force curve slope for isolated wing obtained either from experiment or from linearized-wing theory $\left(\frac{\partial C_N}{\partial \alpha}\right)_W$

$C_{N_{\alpha_{W+B}}}$ normal-force curve slope for wing in combination with cylindrical body $\left(\frac{\partial C_N}{\partial \alpha}\right)_{W+B}$

$c_{N_{\delta_{W+B}}}$ normal-force curve slope for a slender triangular wing in combination with a cylindrical body at 0° angle of attack and the wing deflected with respect to the body center line $\left(\frac{\partial c_N}{\partial \delta}\right)_{W+B}$

c_r tail root chord, feet

l_t distance from wing trailing edge to center of tail root chord, feet

$\frac{l}{q\alpha}$ strip loading per unit angle of attack in terms of the dynamic pressure

M Mach number

q dynamic pressure $\left(\frac{1}{2}\rho V^2\right)$, pounds per square foot

r radial distance from vortex center, feet

Re Reynolds number

s wing semispan, feet

s' semispan of completely rolled-up vortices, feet

s_t	tail semispan, feet
S_W	exposed area of two wing panels, square feet
S_t	gross tail area in one plane (including area within body obtained by extending trailing and leading edges of exposed tail)
T	isolated tail (obtained by extending trailing and leading edges of exposed portion of the tail in combination with the body)
TB	tail–body combination
v	induced velocity at any point in the flow field about a vortex, feet per second
V	free–stream velocity, feet per second
w	component normal to the tail surface of the induced velocity about a vortex, feet per second
W	isolated wing (obtained by extending trailing and leading edges of exposed portion of the wing in combination with the body)
WB	wing–body combination
WBT_o	wing–body–tail combination with the tail surfaces in line with the wing surfaces
WBT_{45}	wing–body–tail combination with the tail surfaces rotated 45° with respect to the wing surfaces
α	angle of attack, degrees
α'	effective tail angle of attack ($\alpha - \epsilon'$), degrees
Γ	circulation
δ	angle of incidence of a wing relative to the body axis, degrees
ϵ	downwash angle at the tail, degrees
ϵ'	effective downwash angle at the tail (tail angle of attack in a uniform stream giving the same lift as the integrated loading due to ϵ obtained from strip theory), degrees
ρ	stream mass density, slugs per cubic foot
φ	angle of bank (positive in clockwise direction looking upstream), degrees

APPARATUS AND TESTS

The experimental portion of the present investigation was conducted in the Ames 6- by 6-foot supersonic wind tunnel at a Mach number of 1.4. This wind tunnel is a closed-return, variable pressure, supersonic wind tunnel in which the Mach number may be varied continuously while the tunnel is in operation. A complete description of the wind tunnel and an analysis of the stream characteristics are given in reference 8. The angle of attack in the present tests was varied in the horizontal plane in order to utilize the most uniform stream conditions.

Model

The model tested (figs. 1 and 2) consisted of a cruciform arrangement of lifting surfaces mounted on a pointed, cylindrical body having a fineness ratio of 16. The forward surfaces of the cruciform wing were of triangular plan form with the leading edges swept back 60° giving an aspect ratio of 2.31. These surfaces had symmetrical, double-wedge airfoils which were 2.90 percent thick at 62.01 percent of the streamwise chord. Each panel was hinged at a point 43 percent of the mean aerodynamic chord. For the present series of tests, the forward surfaces were undeflected with respect to the body center line. The gap between the body and each wing panel was approximately 0.016 inch or about 1/10 percent of the wing span.

The tail fins also were of triangular plan form with leading edges swept back 45° giving an aspect ratio of 4. The tail fins also had symmetrical, double-wedge airfoils with the maximum thickness of 3.02 percent, occuring at 50 percent of the streamwise chord. The tail fins were fixed to the body at zero incidence.

The model was constructed of steel according to the dimensions given in figure 1 and table I and was designed to permit tests of the body alone, body plus wing, body plus tail, or the complete configuration. The complete configuration was tested with the tail interdigitated (tail rotated 45° with respect to the wing) and with the tail in line with the wing.

Support

The model was supported from the rear with a bent sting which was mounted as a cantilever beam on the cross-stream members of the support structure. The relative motion of the two cross-stream beams in combination with the bent sting permitted a test angle-of-attack range of −12° to 22° except in cases where strength limitations would be exceeded.

[redacted]

Measurements

The aerodynamic forces and moments on the model were measured by means of a six-component electrical strain-gage balance located within the cylindrical portion of the body of the model. The unbalance of the electrical circuits of the strain-gage balance, due to the application of loads, was measured by recording light-beam galvanometers. The entire mechanical-electrical system of the balance was calibrated by applying known forces and moments to the model.

The forces acting on each individual panel of the forward variable-incidence wings, which provide longitudinal and lateral control, were measured by flexure type, strain-gage balances in planes perpendicular and parallel to the axis of the model. The moment of these forces about the hinge axis of each wing panel also was measured.

The pressure at the base of the model was determined through the use of the liquid manometer connected to three orifices in the model base.

During the experimental tests, the angle of attack of the model was varied between -12° and 22° except in those instances where the strength limitations of balance and support reduced the maximum angle. The tests were run at angles of bank between 0° and 45° in 11.25° increments. These angles of bank are representative of the complete bank-angle range of the missile in flight because of the four planes of symmetry. To obtain these angles of bank, the model was rotated with respect to the balance. Therefore, for all tests the forces presented are those occurring in the plane in which the angle of attack was varied or in a plane 90° to this plane. In these tests, therefore, the model condition was always noted as an angle of attack in the plane in which the model incidence was varied and an angle of bank of the model wings relative to this plane, the angle of bank considered positive for clockwise rotation as viewed from the rear.

Precision

The accuracy of the experimental data was calculated by considering the sources of possible errors in the determination of the aerodynamic forces, angle of attack, and stream characteristics. The square root of the sum of the squares of the maximum possible errors involved in the determination of a quantity was taken as the final uncertainty in the measurements of the quantity. The final uncertainties at three angles of attack are as follows:

Quantity	Uncertainty for $\alpha = 0^\circ$	Uncertainty for $\alpha = 10^\circ$ to 20°
C_N	±0.0015	±1 (percent of measured value)
C_m	±.002	±2 (percent of measured value)
α	$\pm.15^\circ$	$\pm.1^\circ$
M	.01	.01
Re	.03 million	.03 million

The percentage errors in pitching moment are larger than the errors in normal force because of the numerically smaller values of the pitching-moment coefficient as compared to normal-force coefficient and because of the fact that errors in normal force are reflected in the pitching moment upon transferring the moments to the center-of-gravity position. A precise determination of the angle of attack is dependent in a large part upon an accurate location of the center of pressure of the lifting forces on the model. Near 0° angle of attack, the center-of-pressure position was less accurately known than at higher angles of attack. For this reason, in addition to the fact that the clearances in the six-component balance were such that the model was free to move on the balance approximately $\pm0.1^\circ$, the uncertainty in the angle-of-attack measurements is larger near 0° angle of attack than at higher angles of attack.

The six-component balance was bench calibrated before the tests and was calibrated periodically in the wind tunnel with the model in place. From a total of six such calibrations, the maximum deviation from a mean value in the case of the normal force was ±0.9 percent and ±1.2 percent for the moment gage.

The elastic deformation of the cruciform wing and tail surfaces was recognized as a possible source of error in the wind-tunnel results. Because the leading edges of the wing and tail surfaces were swept back, aeroelastic effects could result in reduced wing and tail lift-curve slopes. Consequently, calculations were made to find the percentage loss in lift from that of completely rigid surfaces which could be expected in the present series of tests. The calculations were based upon the theory of reference 9. The results indicated that the loss in lift for the wing was less than 0.1 percent; the loss for the tail was about 3.5 percent.

RESULTS AND DISCUSSION

As was noted previously, the aerodynamic characteristics of air-to-air missiles are determined to a large extent by the wing-body and wing-wing interference effects. The present investigation is concerned with these effects with the view toward developing methods for determining the contribution of the interference to the over-all longitudinal stability of the missile. For this purpose, it is desirable to subdivide the experimental investigation of the complete missile into a number of investigations of isolated elements and simple combinations of these isolated elements. In the present experiment, since sufficient experimental and theoretical information is available on the wings used for the model, the only isolated element investigated was the body of the missile. The experimental investigation therefore was subdivided as follows:

1. Investigation of the isolated body
2. Investigation of the wing-body combination
3. Investigation of the tail-body combination
4. Investigation of the complete wing-body-tail missile configuration

In the interest of brevity, the analysis of the experimental data obtained is confined to representative cases. The graphical data presented, therefore, are also confined to these cases. The complete experimental results are presented for the reader's use in table II. Throughout this report, the normal-force and pitching-moment coefficients, unless otherwise noted, are based on the exposed area (area of the wing lying outside the body) of two wing panels and on the mean aerodynamic chord of the exposed wing. The use of coefficients so determined applies to the body characteristics as well as the other combinations tested, primarily because of convenience in comparing the contribution of the various elements to the longitudinal stability of the complete configuration of the missile.

All pitching moments are referred to a center-of-gravity position at 59 percent of the mean aerodynamic chord (body station 29.142 as shown in fig. 1). All tests were conducted at a Reynolds number of 1.26 million based on the mean aerodynamic chord.

Isolated Body

The aerodynamic forces and moments acting on the isolated body at an angle of attack, which contribute to the longitudinal stability, can be considered to originate from the following sources:

1. The normal force on the body due to the unseparated potential flow
2. The normal force associated with the separation of the cross-flow boundary layer (reference 10) on the inclined body

The normal forces on the body were determined experimentally through a range of angles of attack up to 22°. These experimental results, together with the pitching-moment coefficients which were also measured, are presented in figure 3 where they are compared with calculated values based on potential-flow theory and on the viscous cross-flow theory of reference 10.

It is evident, from a study of figure 3, that the potential-flow theory originally developed by Munk (reference 11) inadequately predicts the magnitudes of the normal force on the body except for small values of angle of attack. The theory of reference 10, referred to as viscous cross-flow theory, is in much better agreement. It should be noted that the theory of reference 10 includes both the potential cross-flow force on the body as determined from Munk's theory which is confined to that portion of the body which is increasing in size, and the viscous cross force, which is associated with the two-dimensional drag of the body cross sections in a cross-flow velocity of $V \sin \alpha$. The viscous cross-flow theory overestimates to a small degree the magnitude of the normal force up to about 18° angle of attack at which angle the slope of the experimental normal-force curve increased and the normal forces approached those predicted by the viscous theory. The fact that calculated values of the normal-force coefficient were somewhat larger than measured values may have been due to an attenuating influence of favorable pressure gradients on the body nose (reference 12), therefore, less separation may have occurred in this region than the theory assumes. At 18° angle of attack, the cross-flow Mach number is 0.42 at which value, according to figure 9 of reference 10, further increases in cross Mach number are accompanied by significant increases in cross-drag coefficient. The effects of cross Mach number upon the cross-drag coefficient were included in the theoretical results given in figure 3. The maximum cross Reynolds number reached at 22° angle of attack was 0.23 million at a cross Mach number of 0.53.

In the range of angles of attack between 0° and 14°, pitching-moment coefficients for the body alone calculated using viscous cross-flow theory closely approximate measured values. At angles of attack greater than 14°, the slope of the experimental pitching-moment curve first increased and then, at angles of attack greater than about 18°, the pitching-moment coefficients decreased sharply with increasing angle of attack.

In summary, the theory of reference 10 is considered as being of sufficient accuracy to predict the normal forces and pitching moments on the isolated body in the angle-of-attack range up to 20°.

Wing–Body Combination

The aerodynamic forces and moments on the inclined wing–body combination can be subdivided as follows:

1. The forces and moments contributed by the body alone
2. The forces and moments contributed by the isolated wing
3. The forces and moments due to wing–body interference

In the previous section, the aerodynamic forces and moments of the missile body were discussed, and it was shown that the theory of reference 10 gives a close approximation to the experimentally determined forces and moments. Additional experimental and theoretical studies of the lift and moment of triangular wings are available (references 6, 13, 14, and 15) for the estimation of the contribution of the isolated wing.

The magnitude of the interference forces and moments is shown by the comparison in figure 4 wherein the experimentally determined forces and moments are given as functions of the angle of attack and are compared with the algebraic sum of the forces and moments on the isolated elements of the combination as obtained from the present tests of the body and previous tests of a triangular wing of similar thickness (reference 13), appropriately corrected for aspect ratio (reference 14). It will be noted that the wing–body interference is of significant magnitude, amounting to a reduction of about 15 percent in the normal force at all angles of attack and a stabilizing effect on the pitching moments equivalent to a movement of the center of gravity equal to 4 percent of the mean aerodynamic chord. At the present time, a complete theoretical treatment of the interference phenomena does not exist. The theory that does exist is concerned primarily with the interference between the wing and only that portion of the body forward of the wing trailing edge. It is necessary therefore, to treat the estimation of the forces and moments on the wing–body combination in a somewhat approximate manner. The results obtained are also shown in figure 4 and the agreement between the approximate theory and the experiment is found to be quite satisfactory.

This approximate analysis of the interference effects is based on the following considerations:

The forces and moments on the portion of the body ahead of the wing leading–edge juncture are unaltered by the addition of the wing. The presence of the portion of the body adjacent to the wing is considered to influence the aerodynamic forces and moments on the combination in the same manner as the superposition of an infinite cylinder of equal diameter on the isolated wing. The forces and moments on the

portion of the body lying behind the wing trailing edge were estimated and found to be insignificant for the present case.

As was mentioned previously, the study of body lift of reference 12 indicates that there is an attenuating influence of the axial growth of the body nose cross section on the pressure distribution with the net result that the viscous cross-flow forces are not fully developed for this portion of the body. For this reason, the contribution of the nose section of the body to the aerodynamic forces was estimated as being that due to potential flow only.

The contribution of the wing to the forces and moments of the wing-body combination was determined by the method of reference 1. The theoretical considerations of reference 1 are concerned with the application of slender wing-body theory to the estimation of the forces acting on a wing-body combination. The use of slender-body theory permits the reduction of a difficult three-dimensional-flow problem to one of flow in two dimensions about infinitely long cylinders having cross sections which correspond to those of the wing-body combination at various stations. This simplification of the problem, however, results in a restriction of the applicability of the results to wing-body combinations lying well inside the Mach cone. The results of the theory, however, can be applied to the lift of other wing-body combinations by the method used in reference 6, which, in essence, states that the ratio of the lift-curve slope of a wing in combination with an infinite cylindrical body to that of the wing alone as obtained from slender-body theory may be applied to wings of any aspect ratio. This approach may be stated as follows:

$$\frac{C_{N_{\alpha_{W+B}}}}{C_{N_{\alpha_W}}} \times C_{N_{\alpha_W}} = C_{N_{\alpha_{W+B}}} \quad (1)$$

wherein the quotient of the coefficients refers to values determined from slender wing-body theory. This quotient is multiplied by the coefficient noted as $C_{N_{\alpha_W}}$ as determined for the wing either from experimental investigations or from linearized wing theory.

The calculation of the pitching moment of the wing-body combination is also based on the results of reference 1, since both slender-wing theory and linearized-wing theory show the center of pressure on a triangular wing to be located at the center of area, 66.6 percent of the root chord behind the apex of the wing. The theory of reference 1 indicates a rearward movement of the center of pressure to a point at 71 percent of the root chord due to the addition of a body. This value

was used in an estimation of the contribution of the wing plus interference forces to the pitching moments on the wing-body combination.

In summary, the comparison of figure 4 shows that both the normal force and pitching moment determined by the foregoing methods give a very close approximation to the experimentally determined normal forces and pitching moments on the wing-body combination.

The comparison was made for various angles of bank since it was shown in reference 16 that the analysis applies to all angles of bank. The data indicate that, in the present tests, the normal force and pitching moment are invariant with bank angle.

The method used for the analysis of the characteristics of the wing-body combination may be used for other triangular wing-body combinations. It may be necessary to calculate the contribution of the portion of the body behind the wing trailing edge for wings of higher aspect ratio for which the downwash velocities behind the wing are small enough to result in significant cross-flow forces on this portion of the body. Some remarks about this problem are given in reference 17.

Tail-Body Combination

The aerodynamic forces and moments on the inclined tail-body combination, as in the case of the wing-body combination, can be divided into the following:

1. The forces and moments on the isolated body
2. The forces and moments on the isolated tail
3. The forces and moments due to tail-body interference

The magnitude of the interference effects for the tail-body combination is shown by the data of figure 5 wherein the experimentally determined forces and moments for various angles of bank are compared with the sum of the forces and moments for the isolated elements. The aerodynamic characteristics of the body are those determined in the present investigation while those for the tail were taken with appropriate conversion from reference 18 which gives experimental data for an aspect ratio 4 triangular wing, 3 percent thick in streamwise section, geometric characteristics which are very nearly identical to those of the tail of the model of the present experiment. It will be noted that the experimental pitching moments of the isolated components vary nonlinearly with angle of attack. This characteristic is associated primarily with the reduction in tail lift-curve slope with angle of attack shown in reference 18. The comparison of figure 5 shows the interference normal force amounts to 12 percent of the sum of the normal forces contributed by the isolated components at 20° angle of

attack while the interference pitching moment amounts to 26 percent. The interference reduces the magnitude of both the normal force and pitching moment.

The analytical evaluation of the aerodynamic forces and moments for the tail–body combination requires, as in the case of the wing–body combination, considerable approximation as follows:

The forces and moments on the portion of the body ahead of the tail leading-edge juncture are unaltered by the addition of the tail; therefore, the body normal force and pitching moment were calculated by applying the viscous cross-flow theory of reference 10 to the body ahead of the tail leading-edge juncture. The presence of the portion of the body adjacent to the tail is considered to influence the aerodynamic forces and moments on the combination in the same manner as the superposition of an infinite cylinder of equal diameter on the isolated tail.

The contribution of the tail plus the portion of the body adjacent to the tail to the normal force and pitching moment may be analyzed by utilizing slender wing–body theory, with appropriate corrections to account for the fact that the tail cannot be considered slender, as was done in the case of the wing–body combination. However, an additional refinement is necessary.

It will be recalled that in the analysis of the body characteristics (reference 10) the flow around a body of revolution at large angle of attack was shown to exhibit separation characteristics essentially the same as those for a cylinder placed at right angles to a stream of velocity $V \sin \alpha$. The pressure distribution around the periphery of a cross section of the body is nearly identical, therefore, with that for the cylinder at right angles to the stream. Experiments show that when the flow around a cylinder experiences separation, the local peak velocity on the cylinder falls considerably below that for unseparated flow. To facilitate computation it might be assumed that the body upwash in the plane of the tail is reduced in like proportion. This assumption is probably satisfactory provided the ratio of tail span to body diameter is not too large. It is, however, not permissible to utilize the wing–body interference results of reference 1 to calculate the tail–body interference for large angles of attack since for this combination viscous effects must be considered. It is possible, however, to make an approximation by evaluating the effects of body upwash on the tail–body interference as follows:

The slender wing–body theory of reference 1 gives the normal-force-curve slope for a slender triangular wing in combination with an infinite cylindrical body and inclined as a unit as

$$\frac{c_{N_{\alpha_{W+B}}}}{c_{N_{\alpha_W}}} = \left(1 - \frac{a^2}{s^2}\right)^2 \qquad (2)$$

where a is the body radius and s is the wing semispan.

Similar, as yet unpublished, work by Gaynor Adams of the Ames Laboratory for the wing inclined and the body at zero incidence gives the normal-force-curve slope as

$$\frac{c_{N_{\delta_{W+B}}}}{c_{N_{\alpha_W}}} = \frac{2}{\pi}\left[\left(1 + \frac{a^2}{s^2}\right)^2 \tan^{-1}\frac{s}{a} - \pi\frac{a^2}{s^2} + \frac{a}{s}\left(\frac{a^2}{s^2} - 1\right)\right] \qquad (3)$$

where δ refers to the wing incidence relative to the body axis. It should be noted that the coefficients in equations (2) and (3) are based upon the area of the isolated wing (W).

The normal force on the tail and the portion of the body adjacent to the tail will be obtained from the results given by equation 2 and 3. To take into account the viscous cross flow in the present case, a value of the body upwash velocity equal to $0.4\ V \sin\alpha$ was chosen based upon the experimental results of Zahm in reference 19. In applications in which the tail aspect ratio and cross Reynolds number differ markedly from the present tests this numerical value may have to be adjusted. The effects of the reduction of body upwash on the normal-force-curve slope then was written as

$$\left(\frac{c_{N_{\alpha_{T+B}}}}{c_{N_{\alpha_T}}}\right)' = \left(\frac{c_{N_{\alpha_{T+B}}}}{c_{N_{\alpha_T}}} - \frac{c_{N_{\delta_{T+B}}}}{c_{N_{\alpha_T}}}\right) 0.4 + \frac{c_{N_{\delta_{T+B}}}}{c_{N_{\alpha_T}}} \qquad (4)$$

where the coefficients in this case are based upon the area of the isolated tail (T).

The normal-force interference ratio with viscosity effects included (primed quantity of equation 4) has a value of 0.751 for the tail-body combination instead of 0.875 (unprimed ratio) as given by equation 1. The application of this factor to the experimental results of reference 18, appropriately corrected, permits the evaluation of the normal force contributed by the tail in the presence of the body.

The moment about the center of gravity was calculated by assuming the normal force acts at a center of pressure calculated in the same manner as for the wing-body combination in the previous section.

A comparison of the normal force and pitching moment for the tail-body combination computed as outlined above shows satisfactory agreement with experiment in figure 5 for various angles of bank.

Another method of treating the tail–body interference may be developed by assuming that the upwash flow field in the vicinity of the body for the case of viscous cross flow is equivalent to the flow field about an elliptic cylinder of minor axis equal to the diameter of the cross section of the missile body. The major axis of the elliptical cylinder is taken as the distance in the cross-flow plane from the bottom of the missile body to the horizontal streamwise plane which contacts the forward portion of the inclined missile body. With the dimensions of the elliptical cylinder so determined, the results of Nonweiler (reference 20) presenting interference ratios for wing–elliptical–body combinations may be applied.

It is noteworthy that the interference ratio obtained by substituting the flow field about an elliptical cylinder in inviscid flow for the flow field of the circular cylinder in viscous flow agrees closely with the results of equation (4) for the present model at large angles of attack. This method also tends to adjust for the effect of reduced cross–flow separation at small angles of attack.

Complete Configuration

The longitudinal stability of the complete configuration of the missile may be treated by subdividing the aerodynamic forces and moments as follows:

1. The forces and moments contributed by the wing–body combination
2. The forces and moments contributed by the tail–body combination
3. The forces and moments contributed by the interference between the wing in combination with the body and the tail in combination with the body

In the foregoing sections, it has been shown that the aerodynamic forces and moments acting on the wing–body combination and on the tail–body combination can be estimated with satisfactory accuracy. For the complete missile, therefore, the interference resulting from the loads imposed on the tail by the induced flow field of the wing and body is of primary concern.

The interference effects associated with the downwash field of the wing and body are shown in figure 6, which presents experimental normal–force and pitching–moment data obtained for the complete missile configuration at a Mach number of 1.4 for representative angles of bank, and compares the data with the sum of the contributions of the isolated wing–body and the tail (including body–tail interference effects). A study of the data of parts (a), (b), and (c) of figure 6 shows that serious nonlinearities are introduced into the pitching–moment curves through the influence of the downwash field of the wing. The interference effects are found to be most severe for the tail banked 45°

with respect to the wing panels (interdigitated position). For this condition, the pitching-moment curves are nearly linear when the entire missile is at zero angle of bank but become progressively more nonlinear as the angle of bank is increased. At 45° angle of bank, the nonlinearities are so severe as to result in three angles of attack for which aerodynamic balance of the pitching moment is experienced, a condition which is generally undesirable. When the cruciform tail surfaces are placed in line with the wing, the most serious nonlinearities in the pitching-moment curves occur at zero angle of bank, amounting to a significant decrease in the slope of the pitching-moment curve with angle of attack through zero angle of attack. It is evident from the foregoing that the downwash field from the wing introduces interference pitching moments of a most serious nature.

Factors involved in estimating the flow field behind the wing-body combination.- Recent theoretical and experimental studies of the downwash field behind planar triangular wings (references 21 and 22) have shown that for all practical purposes the vortex sheet discharged from the wing trailing edge is essentially rolled up into two concentrated vortex regions for the tail position of the present model for all but small angles of attack. Therefore, it was assumed that the induced effect of the downwash field behind the wing upon the tail of the present configuration could be analyzed by assuming that the vorticity from the wing is rolled up into discrete vortices at the tail location. The vortices were fixed in space by assuming them to originate on the wing trailing edge at approximately 0.8 wing semispan and to lie in the stream direction. The disposition of the vortices so determined is somewhat inaccurate, as is shown in reference 21; however, these approximate positions were verified experimentally by the results of reference 22.

The application of these results to the estimation of the wing-body downwash field in the present problem is subject to some error because of the following two factors:

1. The presence of the cylindrical body of the missile model between the vortices discharged from two opposite wing panels will influence the position of the vortices to some degree. A theoretical estimate of the influence of the body (reference 23), in the present case, shows a negligible influence of the body on the positioning of the vortices in space because of its small size relative to the wing span. The influence of the body, however, may be significantly large if the span of the wing in combination with the body, is much smaller in terms of the body diameter than for the present case and may be of greatest significance, for instance, for canard trimming surfaces. The small influence of the body for the present wing-body combination is shown by the experimental results of reference 22. For further study, reference 4 should be consulted.

2. Application of the results of reference 21, obtained for planar wings, to the cruciform wing of the model of the present investigation for conditions in which both components of the cruciform wing are lifting, will be somewhat in error due to the mutual interaction of the four discharged vortices. This effect is discussed in a subsequent paragraph.

Analysis of the contribution of the tail-body combination in the wing-body downwash field.- The analysis of the pitching moment contributed by the tail is confined to the following two most significant cases:

1. The nonlinear pitching-moment variation with angle of attack experienced when the tail is in line with the model wings and the model is at zero angle of bank
2. The nonlinear variation of pitching moment with angle of attack experienced when the tail is banked 45° with respect to the model wings (interdigitated position) and the entire model is banked 45°

The analysis is confined to these cases in the interest of brevity. The details of the procedures used may have to be modified for other angles of bank.

Tail in line, $\Phi = 0$: In analyzing the first case, tail in line with wings and model at zero bank, the flow field in the region of the tail is assumed to be that associated with two vortices originating at the 0.8 semispan points of the wing and possessing a circulation proportional to the experimental lift carried by the horizontal wing of the cruciform arrangement. (The vertical wing carries no lift in this case since it lies in the plane in which the model angle of attack is varied.)

The tail position is sufficiently removed from the wing so that the bound vorticity in the wing does not influence the induced velocities at the tail. (See reference 24.) Each of the trailing vortices, then, may be considered to extend to infinity in either direction. The induced velocity at any point in the flow field due to the two discharged vortices from the wing may be obtained from the Biot-Savart Law. The loading on the tail in the induced velocity field can be determined by (1) resolving the induced velocities at points along the tail span to obtain the component of velocity perpendicular to the tail surface, and (2) calculating the resulting induced normal force.

The calculation of the induced vertical velocity at the tail surface is simply a problem involving the geometry of the tail and vortex arrangement. Figure 7 shows a diagram of the geometric

considerations used in obtaining the relationship between the induced vertical velocity and the angle of attack. The induced local angle of attack of the tail surfaces can be obtained as the ratio of the induced vertical velocity to the stream velocity. Because of the two-dimensional nature of the flow in the region of the tail, the induced flow angle is constant along any chordwise strip of the tail. The resulting two-dimensional character of the flow used in the above analysis is related to the fact that the rate of distortion of the vortex pattern with distance downstream from the wing is very small.

The loading on the tail can be obtained by applying known methods for calculating the normal force of a planar wing in a nonuniform stream. The methods available for various tail plan forms are discussed in the appendix and the reader is referred to this section for further discussion. It should be noted that a precise calculation of the loading on the tail and the portion of the body adjacent to the tail in the nonuniform flow field behind the wing-body combination presents difficulties because of the interference effects between the tail and the portion of the body adjacent to the tail. To circumvent these difficulties in the present report, recourse was made to the engineering practice of obtaining an effective downwash angle, ϵ', by dividing the theoretical normal force on the tail considered to be a planar wing in a nonuniform flow field by the normal-force-curve slope of the wing in a uniform stream. The pitching moments supplied by the tail and the portion of the body adjacent to the tail may then be obtained by utilizing the pitching moment of the tail, in the presence of the body, as a function of angle of attack determined previously in the analysis of the tail-body combination. The angle of attack to be used is, of course, $(\alpha-\epsilon')$. The pitching-moment characteristics of the complete missile configuration can be obtained by simply adding the contribution due to the tail in the presence of the body, determined as above, to the pitching moments for the wing-body combination at the desired angle of attack.

The analytical results obtained as outlined above are compared with the experimental pitching-moment variation with angle of attack in figure 8. Examination of the data of this figure shows that the analytical method gives a satisfactory estimate of the variation of pitching moment with angle of attack for this condition, tail in line with the wing and the model at 0° angle of bank.

Tail interdigitated, $\varphi = 45^\circ$: As was noted previously, data obtained for the tail interdigitated with the missile at 45° angle of bank show a marked nonlinear variation of pitching moment with angle of attack. The nonlinear character of the pitching-moment curve is attributable to the complex nature of the interference of the cruciform wing and tail arrangement, resulting from the presence of four

regions of concentrated vorticity in the flow field. The contribution of the tail to the pitching moments may be determined analytically in the same manner as was used for the case of the tail in line and missile at zero angle of bank, although the geometric relationships involved in determining the components of induced velocity in the region of the tail are somewhat more complex. A sketch of the geometric arrangement of the tail and the vortices discharged by the wing is shown in figure 9. Although, in this case, both components of the cruciform wing are lifting, the induced velocity in the flow field may be analyzed, to a first order, by considering two independent planar wing systems placed at right angles to one another. As in the previous case, the vortices are assumed to originate at the 0.8-semispan-wing trailing-edge points despite the fact that the span loading is not elliptic. The circulation assigned to each vortex is essentially that which, when taken in conjunction with the assumed vortex positions, gives the normal force acting on each wing panel.

When the missile is banked 45° with respect to the plane in which the angle of attack is varied, each panel of the cruciform wing experiences both a change in an angle of attack and a change in an angle of yaw as the missile angle of attack increases. For planar wing systems which experience no rolling-moment variation with angle of yaw, it is sufficient to determine the lift of each panel from the angle of attack in the plane of symmetry for each component, the angle of attack for each component of the cruciform wing being equal to $\tan^{-1}(\tan \alpha \sin 45^\circ)$. Triangular wings, however, experience a large rolling-moment variation with angle of yaw so that the leading panel of a planar wing carries more lift than the trailing panel. For the cruciform arrangement of present interest, it is evident, therefore, that the two lower panels will carry a greater lift than the two upper panels when the model is banked 45° with respect to the plane in which the angle of attack varies. It is necessary, therefore, in determining the induced flow field to assign the appropriately greater circulation to the two vortices originating on the lower wing panels and a lesser circulation strength to the vortices trailing from the two upper wing panels. The division of load to the leading and trailing panels can be determined, ignoring higher-order wing-interaction effects (reference 25), by applying the linearized theory of yawed lifting triangles at supersonic speeds (reference 26). Figure 10 presents the panel normal forces determined by integrating the loading given by linearized theory (reference 26) over the leading panel and the trailing panel separately of an isolated triangular wing. On this same figure are plotted the experimentally determined panel loadings based on the area of the panel. It will be noted that there is reasonably good agreement between the theoretical and experimental results and that at an angle of attack of 20° the leading panel carries approximately 30 percent more lift than it does at zero angle of yaw, and the trailing panel 30 percent less lift. The vortex strength

assigned to the two lower and to the two upper vortices was based, therefore, on the equivalent division of the experimentally determined lift for the cruciform wing in the presence of the body. In analyzing the induced flow field, the assignment of proper strengths to the upper and lower vortex pairs was found to have a significant influence on the estimated pitching moments due to the tail. The lift of each wing panel and its associated downwash field was replaced by a horseshoe vortex (one for each panel). Since the lifts carried by diametrically opposed panels of the cruciform wing are unequal, the replacement of each wing panel by a vortex filament leaves some net vorticity at the wing root. However, when the net vorticity between the remaining two panels is examined, it is found that this vorticity is of equal but opposite strength which results in a cancellation of the vorticity at the wing root. This cancellation, therefore, leaves only the four vortices originating at the 0.8 semispan points trailing behind the cruciform wing.

The results of the calculations based on the foregoing considerations are compared with the experimentally determined pitching moments in figure 11. It will be noted that there is reasonably good agreement between the analytical pitching moments and the experimental values, although the calculated pitching moments contributed by the tail are somewhat in error at angles of attack from 10° to 14°. It is interesting to note that the shapes of the experimental and theoretical pitching-moment curves agree well. The nearly discontinuous change in pitching moment with angle of attack, shown to occur at 13° angle of attack by the experimental data, is also given by the dashed curve. This point (in the analysis) was found to correspond to the angle of attack for which the horizontal component of the cruciform tail lies in a plane passing through the centers of the two vortices discharged from the lower wing panels. The reader is again referred to the appendix for more detailed consideration of a calculation of the tail pitching moment.

It was realized that the arrangement of the four vortices used in calculating the induced flow field did not include considerations of the mutual interaction of the four vortices on their disposition relative to one another and to the tail. Water-tank experiments which permit the visualization of the flow field behind cruciform wings have shown that the mutual interaction of four vortices significantly distorts the vortex pattern and that the vortices do not trail in the stream direction from their point of origin as was assumed. The deviation of the vortices from the assumed positions, of course, depends on the vortex strength and the relative distances between vortices. For low-aspect-ratio cruciform lifting surfaces, the distortion may be very large.[1] The magnitude of the distortion may be

[1]The discussion here is based on work, as yet unpublished, by Spreiter and Sacks of the Ames Laboratory.

calculated by considering the lateral and vertical velocities induced at the center of one vortex by the action of the other three and by integrating to determine the drift of the vortex center as the flow plane, traveling at stream velocity, proceeds downstream from the wing trailing edge. Essentially such a calculation was performed in the present case for the vortices originating on the two lower wing panels only, since these two vortices contribute the major portion of the induced flow velocities. The result obtained shows that at the tail station the distance between the two lower vortices at 13° angle of attack is 8.5 percent greater than when the vortices are assumed to originate at the 0.8 wing semispan points and to lie in the stream direction. For the purpose of computing the pitching moments, the lateral drift of the two lower vortices was corrected by assuming that the vortices remained fixed as originally assumed, that is, originating at 0.8 semispan and lying in the stream direction, and that the tail span reduced in size with angle of attack in the proper manner as to adjust for the lateral drift of the vortices. The result of the calculation also is shown in figure 11 (by the solid curve) together with the experimental results and the previous calculation which did not consider the lateral drift of the vortices. It will be noted when the lateral motion of the two lower vortices is taken into account, good agreement between the experimental data and the calculated results is found.

It should be emphasized that in the present calculations the two sources of error noted previously, namely, (1) the fact that the influence of the cylindrical body of the missile in contributing to the distortion of the vortex arrangement was disregarded and (2) the incomplete consideration of the effects of the mutual interaction of the vortices in producing distortion of their space arrangement, may be of much greater significance for other missile airframes, particularly those with canard cruciform surfaces.

In addition, no correction to the position of the vortices was made to account for the lateral shift of the center of pressure of the planar components of the banked cruciform wing, due to the combined effective angle of attack and angle of yaw. It appears, however, that the missile body in the present case tends to cause each panel to act independently so that the load distribution over each panel is essentially semi-elliptical though the net load on the lower panels is greater than on the upper panels.

CONCLUDING REMARKS

In previous sections, it has been shown that methods of analysis are available which will permit for the missile investigated a close

estimate of the aerodynamic characteristics of the wing-body combination, tail-body combination, and complete missile configuration including major interference phenomena. The nonlinear pitching-moment characteristics which have long been associated with cruciform wing and tail arrangements are shown to be associated primarily with complex wing-tail interference phenomena which are amenable to calculation.

The results indicate that further research is necessary to improve the accuracy of the calculation of wing-body interference and of the induced flow field behind cruciform wing-body combinations. In particular, the following items need investigation:

1. The influence of the cylindrical body on the distortion of the vortex sheet discharged from the wing trailing edge
2. The mutual interaction of the vortex sheets discharged from each component of the cruciform wing
3. Wing-body interference for cases to which slender wing-body theory does not apply
4. The effects of wing plan form on the distribution of vorticity discharged into the wake of cruciform wings
5. The aerodynamic influence of the elastic deformation of the airframe

Ames Aeronautical Laboratory,
National Advisory Committee for Aeronautics,
Moffett Field, Calif.

APPENDIX

CALCULATIONS OF WING–TAIL INTERFERENCE

Four steps are involved in the calculation of the wing–tail interference:

1. Determination of both the position of the vortices in the vertical plane at the tail and the magnitude of the circulation for each vortex
2. Determination of the local induced flow angle perpendicular to the planar components of the cruciform tail
3. Determination of the effective tail downwash angle
4. Determination of the pitching moment supplied by the tail

The first step, item 1, has been previously discussed in the text of the report; the remainder of the appendix, therefore, will be devoted to the other three steps.

Determination of the Local Induced Flow Angle Perpendicular to the Planar Components of the Cruciform Tail

In the interest of brevity, the analysis of the pitching moment contributed by the tail in the wing downwash field is confined to two cases. The details of the procedures used may have to be modified for other angles of bank and tail orientation. The two problems considered are the following:

1. The missile at zero angle of bank and the tail in line with the wing
2. The missile banked 45° and the tail interdigitated (tail rotated 45° with respect to the wing)

Missile at zero angle of bank and tail in line with the wing.– The necessary geometric relationships involved in the determination of the local downwash angles at the tail for this condition are shown in figure 7. Assuming that the tail position is sufficiently far removed from the wing so that the trailing vortices may be considered to be essentially line vortices extending to infinity in either direction, the induced velocity resulting from the circulation about each vortex is from the Biot–Savart Law

$$v_1 = \frac{\Gamma_1}{2\pi r_1} \quad \text{and} \quad v_2 = \frac{\Gamma_2}{2\pi r_2} \tag{A1}$$

[redacted]

Only the component of these induced velocities perpendicular to the tail surface contributes to the change in tail load, in this case; therefore, only the vertical component of the induced velocity is significant and is given by

$$w = v_1 \cos\left(\tan^{-1}\frac{l_t \sin\alpha}{s' - y}\right) + v_2 \cos\left(\tan^{-1}\frac{l_t \sin\alpha}{s' + y}\right) \qquad (A2)$$

The local downwash angle is

$$\epsilon = \frac{w}{V} = \frac{v_1}{V}\frac{(s' - y)}{r_1} + \frac{v_2}{V}\frac{(s' + y)}{r_2} \qquad (A3)$$

where l_t is the distance from the wing trailing edge to the center of the tail root chord. (To be precise, the length l_t should be the distance from the wing trailing edge to the center of pressure of chordwise strips of the tail and a function of y. To simplify the analysis, however, this distance was approximated as a constant value.)

By means of the Kutta-Joukowski Theorem, the strength of the vortices may be related to the lift of the wing-body combination as

$$|\Gamma_1| = |\Gamma_2| = \frac{N_{WB}}{\rho V 2 s'} = \frac{C_{N_{\alpha_{WB}}}\ \alpha\ (\frac{1}{2}\rho V^2)\ S_W}{\rho V 2 s'} \qquad (A4)$$

Substituting equations (A4) and (A1) into equation (A3), the local downwash angle becomes

$$\epsilon = \frac{C_{N_{\alpha_{WB}}}\ \alpha\ S_W}{8\pi s'}\left(\frac{s' - y}{r_1^2} + \frac{s' + y}{r_2^2}\right) \qquad (A5)$$

where

r distance from the center of the vortex to the chordwise strip of the tail

r_1^2 $(l_t \sin\alpha)^2 + (s' - y)^2$

r_2^2 $(l_t \sin\alpha)^2 + (s' + y)^2$

S_W exposed area of two wing panels

α angle of attack

$C_{N_{\alpha_{WB}}}$ experimental value for the slope of the normal-force curve for the wing-body combination with the body normal force in potential flow subtracted (based on the exposed area of two wing panels)

Equation (A5) defines the spanwise variation of the downwash angle at the tail location.

Missile at 45° angle of bank and tail interdigitated.- When the components of the cruciform wing of the missile are banked at 45° with respect to the plane in which the angle of attack is varied, the local downwash angle at the tail may be determined analytically in the same manner as was used for the case of the tail in line and the missile at zero bank angle. The geometric relationships involved are somewhat more complex, however, because of the presence of four vortices in the flow field. A sketch of the geometric arrangement of the tail and the vortices discharged by the wing is shown in figure 9.

Again, the strength of each vortex can be related to the normal force on the four panels composing the cruciform wing by means of the Kutta-Joukowski Theorem. The strength of each vortex is

$$\Gamma_n = \frac{N_n}{\rho V s'} = \frac{C_{N_n} \left(\frac{1}{2} \rho V^2\right) S_W}{\rho V s'} \tag{A6}$$

where n = 1, 2, 3, 4 refers to each wing panel and to the tip vortices trailing behind each panel; N_n is the normal force on each panel; and C_{N_n}, is the normal-force coefficient on each panel.

From the geometric relations shown in figure 9, the spanwise variation of the downwash angle at the tail location induced by vortices 1 and 2 is

$$\epsilon_1 = \frac{\Gamma_1}{2\pi V} \frac{(s' \cos \varphi - y)}{(l_t \sin \alpha - s' \sin \varphi)^2 + (s' \cos \varphi - y)^2}$$

$$\epsilon_2 = \frac{\Gamma_2}{2\pi V} \frac{(s' \cos \varphi + y)}{(l_t \sin \alpha + s' \sin \varphi)^2 + (s' \cos \varphi + y)^2} \tag{A7}$$

Substituting for Γ_1 and Γ_2 from equation (A6), the spanwise variation of the downwash angle due to the induced velocity field from vortices 1 and 2 is

$$\epsilon = \frac{C_{N_1} S_W (s' \cos \varphi - y)}{4\pi s'[(l_t \sin \alpha - s' \sin \varphi)^2 + (s' \cos \varphi - y)^2]} + \frac{C_{N_2} S_W (s' \cos \varphi + y)}{4\pi s'[(l_t \sin \alpha + s' \sin \varphi)^2 + (s' \cos \varphi + y)^2]} \quad \text{(A8)}$$

where C_{N_1} and C_{N_2} are the normal-force coefficients on panels 1 and 2 based upon the exposed area of two wing panels. These coefficients were obtained by dividing the experimentally determined normal force for the cruciform wing and body combination (figs. 3 and 4) proportionally to the lift on the leading panel and trailing panels of the banked cruciform wing as shown in figure 10. This procedure was discussed in the text of the report.

From symmetry, of course, the local induced downwash angle due to vortices 3 and 4 may be determined by simply substituting $-y$ for y in equation (A8).

Determination of the Effective Downwash Angle at Tail

Before discussing the calculation of the effective downwash angle in the present case, it is perhaps desirable to discuss the various methods available for estimating tail loads in nonuniform flow fields. A number of theoretical analyses for determining the loading of planar wings in nonuniform flow fields are available, ranging from modified strip theories to solutions exact within the limitations of the linearized theory. The methods fall into certain categories determined by the relationship of the sweep of the Mach lines to the sweep of elements of the wings as follows:

1. Wings lying near the center of the Mach cone (slender wing and wing-body theories)
2. Wings with subsonic leading edges (application of reversed flow theorems)
3. Wings with supersonic edges

Wings lying near the center of the Mach cone.— In this category, several new theoretical treatments are available. In particular, in a recent article in the Journal of the Aeronautical Sciences (reference 27), Morikawa and Puckett arrived at the solution for the spanwise lift influence function for two chordwise strips of infinitesimal width, at small angles of attack, and symmetrically disposed on each side of the vertical center plane. The result obtained shows the lift

associated with the strips to vary with the spanwise position of the strips in the same manner as the spanwise loading for the slender wing or slender wing–body combination at angle of attack. Similar work by Adams (reference 28) for slender wings gives results which may be applied to calculations for asymmetric flow fields.

Further work of great usefulness in this category has been done by Lomax and Byrd (reference 29) for the case of slender wings and slender wing–body combinations in the presence of distributed vortex sheets as well as discrete vortices. The results are given in closed form.

Sufficient theory exists, therefore, to permit the calculation of tail loads for tail plan forms lying well within the Mach cone.

Wings with subsonic edges.– No exact solutions have been published in this category. Approximate solutions exist in the form of strip theories (references 9 and 30), and exact solutions can be obtained in cases where there is no interaction between leading edges. However, it has been pointed out by several investigators that exact solutions for the load associated with an inclined chordwise strip of a triangular wing can be deduced by applying the reversed-flow theorems of references 31, 32, 33, and 34. The resulting theorem is as follows:

> The influence of the deflection of a chordwise strip of a wing on the loading of the wing is equivalent to the influence exerted on the loading of the strip as the result of placing the entire wing at the same angle of attack in reversed flow.

The result is, therefore, that the spanwise influence function, as defined by Alden and Schindel in reference 35, is identical to the span load distribution of the triangular wing in reversed flow. It appears, therefore, that exact solutions for wings in nonuniform flows can be obtained when reversed flow theorems are applied.

Wings with supersonic edges.– Considerable information exists for wings swept ahead of the Mach line (references 35 and 36). Exact solutions are available in most cases and both spanwise and chordwise stream nonuniformities may be treated.

In the present report the method of reference 36 was applied to the calculation of the tail loading to determine the effective downwash angle at the tail since the tail leading edges are sonic. The effective downwash angle at the tail was calculated as

$$\epsilon' = \frac{2}{s_t}\int_0^{s_t} C_r\left(1-\frac{y}{s_t}\right)\epsilon \, dy \qquad \text{(A9)}$$

[redacted]

By substitution of the expression for the spanwise variation of the downwash angle at the tail location given by equations (A5) and (A8), the effective downwash angles for the two cases considered become

For BWT_o, $\varphi = 0^o$:

$$\epsilon' = \frac{C_{N_{\alpha_{WB}}} \alpha S_W}{4\pi s' S_t} \left\{ \int_o^{s_t} C_r \left(1 - \frac{y}{s_t}\right) \left[\frac{(s' - y)}{(l_t \sin \alpha)^2 + (s' - y)^2} + \frac{(s' + y)}{(l_t \sin \alpha)^2 + (s' + y)^2} \right] dy \right\} \tag{A10}$$

For BWT_{45}, $\varphi = 45^o$:

$$\epsilon' = \frac{S_W}{\pi s' S_t} \left\{ \int_o^{s_t} C_r \left(1 - \frac{y}{s_t}\right) \left[\frac{C_{N_1} (s' \cos \varphi - y)}{(l_t \sin \alpha - s' \sin \varphi)^2 + (s' \cos \varphi - y)^2} + \frac{C_{N_2} (s' \cos \varphi + y)}{(l_t \sin \alpha + s' \sin \varphi)^2 + (s' \cos \varphi + y)^2} \right] dy \right\} \tag{A11}$$

The above equations may be evaluated analytically to obtain closed expressions for the effective downwash angles at the tail location. The final expressions are somewhat cumbersome, however, and for this reason have not been included.

Determination of the Pitching Moment Supplied by the Tail

Utilizing the effective downwash angles previously calculated, the contribution of the tail and the portion of the body adjacent to the tail to the pitching moment of the complete configuration can be obtained from the experimental and/or theoretical pitching-moment curves for the tail-body combination and the body-alone results (figs. 5 and 3, respectively), as

$$C_{m_t} = C_{m_{TB-B}} f(\alpha - \epsilon') \tag{A12}$$

The pitching moment for the complete configuration may be obtained by adding the contribution of the tail, as obtained in each case by the procedure indicated in equation (A12), to the appropriate experimental or theoretical values of the pitching moment for the wing-body combination given in figure 4.

In the foregoing analysis, experimental data for the aerodynamic forces and moments upon the isolated components of the missile were used in order to suppress, insofar as possible, redundant errors that might appear due to discrepancies between theoretical calculations of these forces and moments and experiment. It should be pointed out that the use of these experimental data does not detract from the generality of the analysis, since the results contained in the body of the report show that the longitudinal stability characteristics of the isolated components of the present model can be predicted with reasonable accuracy. A comparison of the measured longitudinal stability characteristics of the complete configuration and the calculations for the two configurations considered (shown in figs. 8 and 11) appear to confirm the appropriateness of the assumption that the vortices behind the cruciform wing are completely rolled up at the tail location.

REFERENCES

1. Spreiter, John R.: Aerodynamic Properties of Slender Wing-Body Combinations at Subsonic, Transonic, and Supersonic Speeds. NACA Rep. 962, 1950. (Formerly NACA TN 1662)

2. Adams, Gaynor J.: Theoretical Damping in Roll and Rolling Effectiveness of Slender Cruciform Wings. NACA TN 2270, 1951.

3. Ferrari, C.: Interference Between Wing and Body at Supersonic Speeds – Theory and Numerical Application. Jour. Aero. Sci., vol. 15, no. 6, June 1948, pp. 317 – 336.

4. Lagerstrom, P. A., and Graham, M. E.: Aerodynamic Interference in Supersonic Missiles. Douglas Aircraft Co. Rep. SM-13743, July 1950.

5. Stewart, H. J., and Meghreblian, R. V.: Body-Wing Interference in Supersonic Flow. GALCIT/JPL PR 4-99, June 1949.

6. Nielsen, Jack N., Katzen, Elliott D., and Tang, Kenneth K.: Lift and Pitching-Moment Interference Between a Pointed Cylindrical Body and Triangular Wings of Various Aspect Ratios at Mach Numbers of 1.50 and 2.02. NACA RM A50F06, 1950.

7. Cramer, R. H.: Interference Between Wing and Body at Supersonic Speeds, Part V, Phase I – Wind Tunnel Tests Correlated with the Linearized Theory, Cornell Aeronautical Laboratory Rpt. CAL/CM-597, October 1950.

8. Frick, Charles W., and Olson, Robert N.: Flow Studies in the Asymmetric Adjustable Nozzle of the Ames 6- by 6-Foot Supersonic Wind Tunnel. NACA RM A9E24, 1949.

9. Frick, Charles W., and Chubb, R. S.: The Longitudinal Stability of Elastic Swept Wings at Supersonic Speeds. NACA Rep. 965, 1950. (Formerly NACA TN 1811)

10. Allen, H. Julian: Estimation of the Forces and Moments Acting on Inclined Bodies of Revolution of High Fineness Ratio. NACA RM A9I26, 1949.

11. Munk, Max M.: The Aerodynamic Forces on Airship Hulls. NACA Rep. 184, 1924.

12. Allen, H. Julian, and Perkins, Edward W.: Characteristics of Flow Over Inclined Bodies of Revolution. NACA RM A50L07, 1951.

13. Heitmeyer, John C., and Smith, Willard G.: Lift, Drag, and Pitching Moment of Low Aspect Ratio Wings at Subsonic and Supersonic Speeds – Plane Triangular Wing of Aspect Ratio 2 With NACA 0003–63 Section. NACA RM A50K24a, 1951.

14. Stewart, H. J.: The Lift of a Delta Wing at Supersonic Speeds. Quart. App. Math., vol. IV, no. 3, Oct. 1946, pp. 246 – 254.

15. Brown, Clinton E.: Theoretical Lift and Drag of Thin Triangular Wings at Supersonic Speeds. NACA Rep. 839, 1946. (Formerly NACA TN 1183)

16. Spreiter, John R.: Aerodynamic Properties of Cruciform-Wing and Body Combinations at Subsonic, Transonic, and Supersonic Speeds. NACA Rep. 962, 1950. (Formerly NACA TN 1897)

17. Lagerstrom, P. A., and Graham, M. E.: Remarks on Low-Aspect-Ratio Configurations in Supersonic Flow. Jour. Aero. Sci., vol. 18, no. 2, Feb. 1951, pp. 91 – 97. (Also issued as: CIT Pub. 269)

18. Heitmeyer, John C.: Lift, Drag, and Pitching Moment of Low-Aspect-Ratio Wings at Subsonic and Supersonic Speeds – Plane Triangular Wing of Aspect Ratio 4 With 3-Percent Thick, Biconvex Section. NACA RM A51D30, 1951.

19. Zahm, A. F.: Flow and Drag Formulas for Simple Quadrics. NACA Rep. 253, 1927.

20. Nonweiler, T.: The Theoretical Lift and Pitching Moment of a Highly-Swept Delta Wing on a Body of Elliptic Cross Section. Tech. Note No. Aero 2055, British R.A.E., 1950.

21. Spreiter, John R., and Sacks, Alvin H.: The Rolling Up of the Trailing Vortex Sheet and Its Effect on the Downwash Behind Wings. Jour. Aero. Sci., vol. 18, no. 1, January 1951.

22. Wetzel, Benton E., and Pfyl, Frank A.: Measurements of Downwash and Sidewash Behind Cruciform Triangular Wings at Mach Number 1.4. NACA RM A51B20, 1951.

23. Milne-Thomson, L. M.: Theoretical Hydrodynamics. Macmillan, London, 1938.

24. Heaslet, Max. A., and Lomax, Harvard: The Calculation of Downwash Behind Supersonic Wings With an Application to Triangular Plan Forms. NACA Rep. 957, 1950. (Formerly NACA TN 1620)

25. Maple, C. G., and Synge, J. L.: Aerodynamic Symmetry of Projectiles. Quart. App. Math., vol. VI, no. 4, January 1949, pp. 345 – 366.

26. Jones, Arthur L., and Alksne, Alberta: The Load Distribution Due to Sideslip on Triangular, Trapezoidal, and Related Plan Forms in Supersonic Flow. NACA TN 2007, 1950.

27. Morikawa, G. K., and Puckett, A. E.: Equivalence of the Spanwise Lift Distribution to the Spanwise Lift-Influence Function for Slender Wings and Wing Bodies. Jour. Aero. Sci., vol. 18, no. 7, July, 1951, pp. 503 – 504.

28. Adams, Gaynor J.: Theoretical Damping in Roll and Rolling Effectiveness of Slender Cruciform Wings. NACA TN 2270, 1951.

29. Lomax, Harvard, and Byrd, Paul F.: Aerodynamic Characteristics of Airplane Configurations Involving Slender Wing-Tail-Body Combinations. NACA TN 2554, 1951.

30. Graham, M. E.: Some Linearized Computations of Supersonic Wing-Tail Interference. Douglas Rept. No. SM-13430, Dec. 1948.

31. Jones, R. T.: The Minimum Drag of Thin Wings in Frictionless Flow. Jour. Aero. Sci., vol. 18, no. 2, Feb. 1951, pp. 75 – 81.

32. Ursell, F., and Ward, G. N.: On Some General Theorems in the Linearized Theory of Compressible Flow. Quart. Jour. of Mech. and App. Math., vol. III, pt. 3, 1950, pp. 326 – 348.

33. Munk, M. M.: The Reversal Theorem of Linearized Supersonic Airfoil Theory. Jour. App. Phys., vol. XXI, no. 2, Feb. 1950. (Naval Ordnance Lab. Memo. 9624, July 26, 1948.)

34. Brown, Clinton E.: The Reversibility Theorem for Thin Airfoils in Subsonic and Supersonic Flow. NACA Rep. 986, 1950. (Formerly NACA TN 1944)

35. Alden, Henry L., and Schindel, Leon H.: The Calculation of Wing Lift and Moments in Nonuniform Supersonic Flows. M.I.T. Meteor Rept. No. 53, May 1950.

36. Lagerstrom, P. A., and Van Dyke, M. D.: General Considerations About Planar and Non-Planar Lifting Surfaces. Douglas Aircraft Company Rept. SM 13432, June 1949.

TABLE I.- MODEL DIMENSIONAL DATA

Body	
Over-all length, inches	57.31
Distance from nose tip to:	
End of ogival nose section (beginning of constant section), inches	22.50
Leading edge of main fin (intersection with body), inches	20.92
Trailing edge of main fin, inches	32.22
Leading edge of tail fin (intersection with body), inches	51.77
Trailing edge of tail fin, inches	57.07
Center of gravity position, inches	29.14
Diameter of constant section, inches	3.60

Fins	Main	Tail
Thickness (percent local chord), percent	2.90	3.02
Location of maximum thickness (percent chord), percent	62.01	50.00
Over-all span, inches	16.68	14.19
Root chord (theoretical at body center line), inches	14.45	7.10
Tip chord	0.00	0.00
Chord at fin-body intersection, inches	11.31	5.30
Hinge-line body station, inches	27.93	--
Theoretical vertex angle at body center line, degrees	30.0	45.0
Gross area, two fins, inches squared	120.53	50.40
Mean aerodynamic chord of gross area, inches	9.63	4.73
Exposed area, two fins, inches squared	73.87	28.08
Mean aerodynamic chord of exposed area, inches	7.54	3.53

NACA

TABLE II.- CHARACTERISTICS OF VARIOUS CONFIGURATIONS

(a) Body Alone

α (deg)	C_N	C_m	α (deg)	C_N	C_m
-4.0	-0.0370	-0.0175	10.1	0.0930	0.0841
-2.0	-.0169	-.0134	12.2	.1222	.1044
0	.0001	-.0031	14.2	.1587	.1222
2.0	.0151	.0088	16.3	.1962	.1560
4.0	.0291	.0300	18.3	.2470	.1771
6.1	.0449	.0546	20.4	.3351	.1875
8.1	.0674	.0679	22.5	.4637	.1457

TABLE II.- CONTINUED

(b) Wing Plus Body

φ = 0°			φ = 11.25°			φ = 22.5°			φ = 33.75°			φ = 45°		
α (deg)	C_N	C_m	α (deg)	C_N	C_m	α (deg)	C_N	C_m	α (deg)	C_N	C_m	α (deg)	C_N	C_m
-11.3	-0.8495	-0.2803	-11.3	-0.8354	-0.2735	-11.3	-0.8553	-0.2550	-9.1	-0.6835	-0.2423	-11.3	-0.8542	-0.2697
-9.1	-.6870	-.2101	-9.1	-.6703	-.2199	-9.1	-.6809	-.2031	-7.0	-.5063	-.1849	-9.1	-.6935	-.2102
-7.0	-.5158	-.1558	-7.0	-.5023	-.1675	-7.0	-.5071	-.1536	-4.8	-.3364	-.1268	-7.0	-.5123	-.1589
-4.8	-.3443	-.1085	-4.8	-.3386	-.1142	-4.8	-.3415	-.1024	-2.6	-.1734	-.0690	-4.8	-.3350	-.1016
-2.6	-.1742	-.0591	-2.6	-.1758	-.0625	-2.6	-.1770	-.0542	-0.4	-.0299	-.0087	-2.6	-.1688	-.0520
-.4	-.0280	-.0053	-.4	.0240	-.0076	-.4	-.0302	-.0061	2.2	.1458	.0666	-.4	-.0301	-.0073
2.3	.1500	.0570	2.2	.1495	.0577	2.2	-.1466	.0595	4.5	.3172	.1202	2.2	.1495	.0707
4.5	.3356	.1036	4.5	.3275	.1117	4.4	.3234	.1098	6.7	.4916	.1856	4.6	.3173	.1217
6.6	.5130	.1431	6.7	.5016	.1641	6.6	.5032	.1584	8.8	.6689	.2338	6.7	.4988	.1727
8.8	.6867	.1856	8.8	.6732	.2100	8.8	.6759	.2153	11.0	.8421	.2947	8.8	.6748	.2338
11.0	.8573	.2676	11.0	.8425	.2599	11.0	.8421	.2670	13.2	1.0110	.3412	11.0	.8463	.2764
13.1	1.0223	.3033	13.2	1.0145	.2979	13.2	1.0057	.3066	15.4	1.1849	.3975	13.2	1.0209	.3244
15.3	1.1970	.3489	15.4	1.1716	.3647	15.3	1.1683	.3606	17.5	1.3557	.4462	15.4	1.1876	.3746
17.5	1.3616	.3906	17.5	1.3330	.4168	17.5	1.3378	.4095	19.7	1.5475	.5020	17.5	1.3730	.4216
19.6	1.5468	.4219	19.6	1.4832	.4608	19.7	1.4985	.4726	---	---	---	19.7	1.5620	.4843
21.7	1.7097	.4721	21.8	1.6523	.5109	21.8	1.6620	.5409	---	---	---	---	---	---

TABLE II.— CONTINUED

(c) Tail Plus Body

$\varphi = 0°$			$\varphi = 11.25°$			$\varphi = 22.5°$			$\varphi = 33.75°$			$\varphi = 45°$		
α (deg)	C_N	C_m	α (deg)	C_N	C_m	α (deg)	C_N	C_m	α (deg)	C_N	C_m	α (deg)	C_N	C_m
-9.8	-0.4055	0.969	-9.8	-0.4088	-0.991	-9.9	-0.4192	1.005	-9.8	-0.4187	0.989	-9.8	-0.4182	1.001
-7.8	-.3250	.789	-7.8	-.3288	-.803	-7.8	-.3306	.816	-7.8	-.3331	.798	-7.8	-.3317	.811
-5.8	-.2437	.588	-5.8	-.2456	-.507	-5.8	-.2468	.613	-5.8	-.2487	.595	-5.8	-.2480	.609
-3.8	-.1630	.384	-3.8	-.1634	-.401	-3.8	-.1639	.405	-3.8	-.1657	.390	-3.8	-.1654	.395
-1.8	-.0809	.179	-1.8	-.0802	-.183	-1.8	-.0810	.188	-1.8	-.0830	.179	-1.8	-.0817	.179
-.3	-.0175	.023	-.3	-.0160	-.027	-.3	-.0163	.029	-.3	-.0176	.021	-.3	-.0189	.021
.3	.0119	-.022	.3	.0110	-.025	.3	.0120	-.028	.5	.0110	-.045	.5	.0110	-.039
1.8	.0749	-.180	1.8	.0753	-.182	1.8	.0771	-.187	1.8	.0741	-.177	1.8	.0771	-.181
3.8	.1571	-.398	3.8	.1598	-.405	3.8	.1621	-.410	3.8	.1582	-.399	3.8	.1596	-.401
5.8	.2399	-.606	5.8	.2421	-.611	5.8	.2448	-.619	5.8	.2411	-.608	5.8	.2415	-.611
7.8	.3193	-.795	7.8	.3237	-.805	7.8	.3265	-.811	7.8	.3236	-.804	7.8	.3260	-.814
9.9	.3995	-.970	9.8	.4097	-.989	9.8	.4073	-.989	9.8	.4094	-.997	9.8	.4102	-1.003
11.9	.4803	-1.134	11.9	.4891	-1.154	11.9	.4922	-1.163	11.9	.4952	-1.174	11.7	.4924	-1.173
13.9	.5631	-1.283	13.9	.5718	-1.303	13.9	.5784	-1.322	13.9	.5833	-1.342	13.9	.5796	-1.343
15.9	.6505	-1.422	15.9	.6555	-1.437	15.9	.6661	-1.470	15.9	.6789	-1.511	15.9	.6737	-1.515
18.0	.7356	-1.532	17.9	.7442	-1.559	17.9	.7560	-1.597	17.9	.7707	-1.647	17.9	.7738	-1.660
20.0	.8410	-1.623	20.0	.8533	-1.647	20.0	.8672	-1.679	20.0	.8722	-1.707	20.0	.8851	-1.752

NACA

TABLE II – CONTINUED

(d) Complete Configurations

WBT_o														
$\varphi = 0°$			$\varphi = 11.25°$			$\varphi = 22.5°$			$\varphi = 33.75°$			$\varphi = 45°$		
α (deg)	C_N	C_m	α (deg)	C_N	C_m	α (deg)	C_N	C_m	α (deg)	C_N	C_m	α (deg)	C_N	C_m
-11.4	-1.1153	0.5921	-11.3	-1.0987	0.5693	-11.3	-1.0934	0.5247	-11.3	-1.0935	0.4620	-11.2	-1.0696	0.4321
-9.3	-.9020	.4393	-9.2	-.8718	.4150	-9.2	-.8815	.3990	-9.1	-.8666	.3337	-9.1	-.8709	.3305
-7.2	-.6742	.2884	-7.1	-.6614	.2783	-7.1	-.6681	.2738	-7.0	-.6524	.2186	-6.9	-.6521	.2210
-5.0	-.4561	.1634	-4.9	-.4449	.1620	-4.9	-.4489	.1570	-4.8	-.4363	.1238	-4.8	-.4323	.1233
-2.7	-.2348	.0651	-2.6	-.2285	.0674	-2.6	-.2321	.0674	-2.6	-.2337	.0557	-2.6	-.2285	.0624
-.4	-.0392	.0283	-0.3	-.0152	.0045	-0.3	-.0140	.0270	-0.3	-.0387	.0200	-.3	-.0310	.0113
2.2	.1742	-.0248	2.3	.1894	-.0376	2.3	.1826	-.0236	2.3	.1650	-.0191	2.3	.1795	-.0301
4.5	.3967	-.1245	4.5	.3957	-.1150	4.5	.3894	-.0987	4.5	.3765	-.0838	4.5	.3850	-.1028
6.7	.6163	-.2488	6.7	.6137	-.2294	6.7	.6105	-.2039	6.7	.5942	-.1784	6.6	.5956	-.1927
8.9	.8363	-.3945	8.9	.8321	-.3643	8.9	.8248	-.3223	8.9	.8068	-.2816	8.8	.8186	-.2750
11.0	1.0651	-.5578	11.0	1.0616	-.5156	11.1	1.0503	-.4553	11.0	1.0283	-.3978	11.0	1.0342	-.3775
13.1	1.3001	-.7183	13.2	1.2794	-.6559	13.2	1.2656	-.5881	13.1	1.2487	-.5189	13.1	1.2598	-.5388
15.2	1.5044	-.8523	15.3	1.4732	-.7718	15.3	1.4865	-.7149	15.3	1.4490	-.6213	15.2	1.4738	-.6447
17.3	1.6877	-.9604	17.4	1.6938	-.9052	17.5	1.6771	-.7691	17.4	1.6499	-.7005	17.3	1.6840	-.7294
19.5	1.9088	-1.0981	19.5	1.8834	-1.0082	19.6	1.8550	-.8250	18.1	1.7282	-.7305	19.4	1.8795	-.7746
21.6	2.1347	-1.1972	---	---	---	---	---	---	---	---	---	21.6	2.0834	-.8390

TABLE II.- CONCLUDED

(d) Concluded

WBT_{45}															
$\varphi = 0°$			$\varphi = 11.25°$			$\varphi = 22.5°$			$\varphi = 33.75°$			$\varphi = 45°$			
α (deg)	C_N	C_m	α (deg)	C_N	C_m	α (deg)	C_N	C_m	α (deg)	C_N	C_m	α (deg)	C_N	C_m	
-11.3	-1.0939	0.5341	-11.3	-1.0828	0.5115	-11.4	-1.0477	0.3745	-11.4	-1.0047	0.1338	-11.4	-0.9729	0.0440	
-9.2	-.8820	.4152	-9.2	-.8746	.4109	-9.2	-.8611	.3430	-9.2	-.8265	.2018	-9.2	-.8173	.1712	
-7.0	-.6779	.3314	-7.0	-.6719	.3349	-7.0	-.6720	.3086	-7.0	-.6453	.2260	-7.0	-.6502	.2485	
-4.8	-.4724	.2545	-4.8	-.4648	.2587	-4.8	-.4724	.2484	-4.8	-.4576	.2060	-4.7	-.4556	.2265	
-2.6	-.2561	.1643	-2.5	-.2447	.1634	-2.6	-.2624	.1659	-2.6	-.2614	.1521	-2.5	-.2575	.1467	
-0.3	-.0138	.0275	-0.2	-.0019	.0219	-0.3	-.0174	-.0004	-0.3	-.0337	.0299	-0.3	-.0373	.0351	
2.3	.2136	-.1072	2.3	.2124	-.1150	2.3	.2036	-.1015	2.3	.1912	-.0999	2.3	.2029	-.1082	
4.6	.4392	-.2258	4.5	.4309	-.2214	4.5	.4260	-.2039	4.5	.4093	-.1925	4.5	.4202	-.2090	
6.7	.6447	-.3142	6.7	.6350	-.2966	6.7	.6326	-.2624	6.7	.6147	-.2326	6.6	.6229	-.2488	
8.9	.8481	-.3994	8.9	.8335	-.3515	8.9	.8138	-.2572	8.9	.7882	-.1692	8.9	.7910	-.1915	
11.0	1.0595	-.5122	11.1	1.0334	-.4154	11.1	.9908	-.2182	11.1	.9601	-.0874	11.0	.9561	-.0818	
13.2	1.2843	-.6538	13.2	1.2407	-.5163	13.3	1.1978	-.2821	13.3	1.1456	-.0715	13.2	1.1353	.0102	
15.3	1.4896	-.8005	15.3	1.4146	-.6105	15.4	1.4049	-.3830	15.4	1.3729	-.2762	15.2	1.3887	-.2589	
17.5	1.6984	-.9386	17.5	1.6230	-.7389	17.5	1.6198	-.5658	17.5	1.5956	-.5067	17.3	1.6404	-.5074	
- - -	- - -	- - -	- - -	- - -	- - -	- - -	- - -	- - -	18.2	1.6805	-.5827	19.5	1.8582	-.6952	
- - -	- - -	- - -	- - -	- - -	- - -	- - -	- - -	- - -	- - -	- - -	- - -	21.5	2.1001	-.8823	

NACA

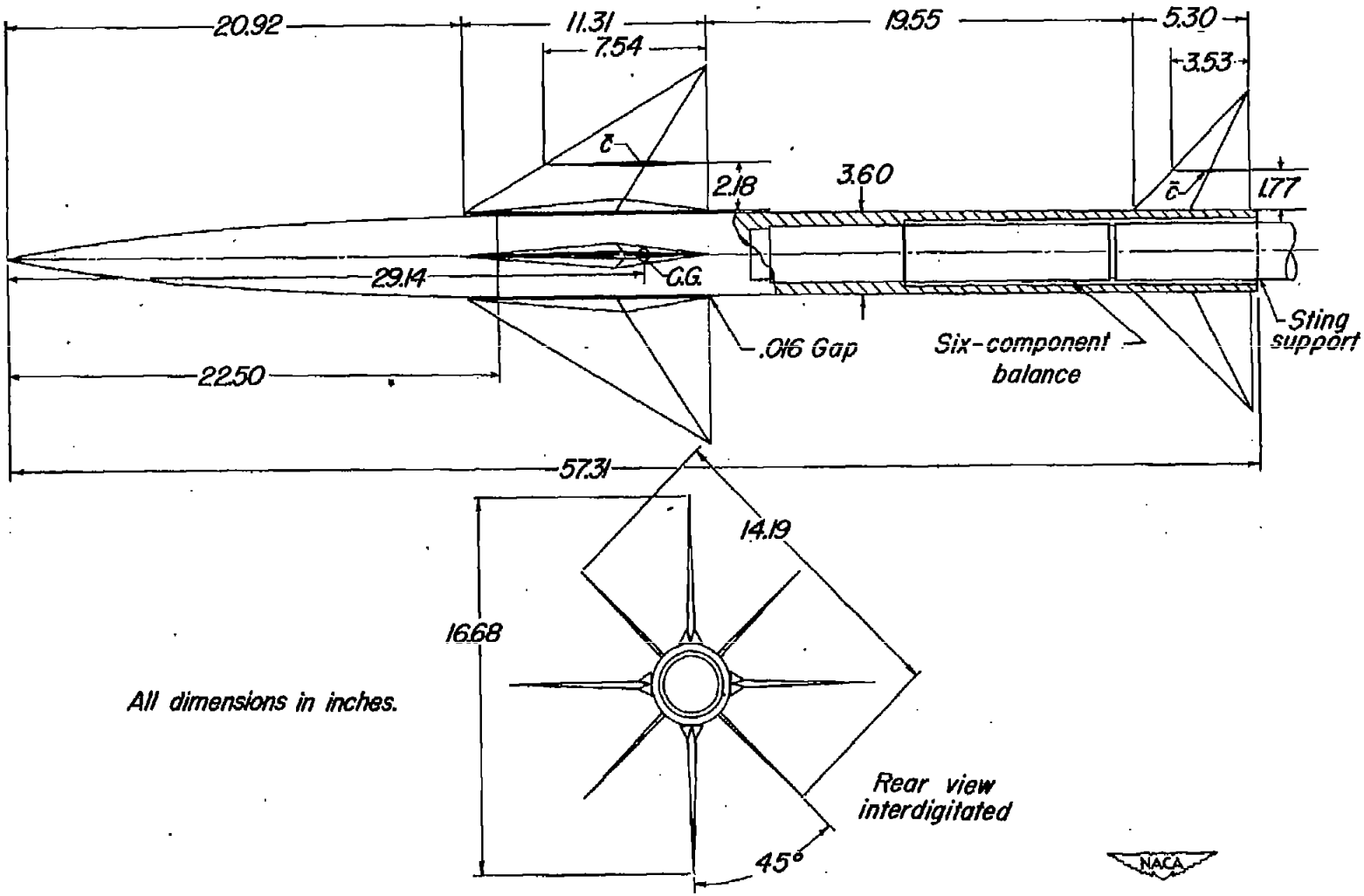

Figure 1.-Dimensions of model.

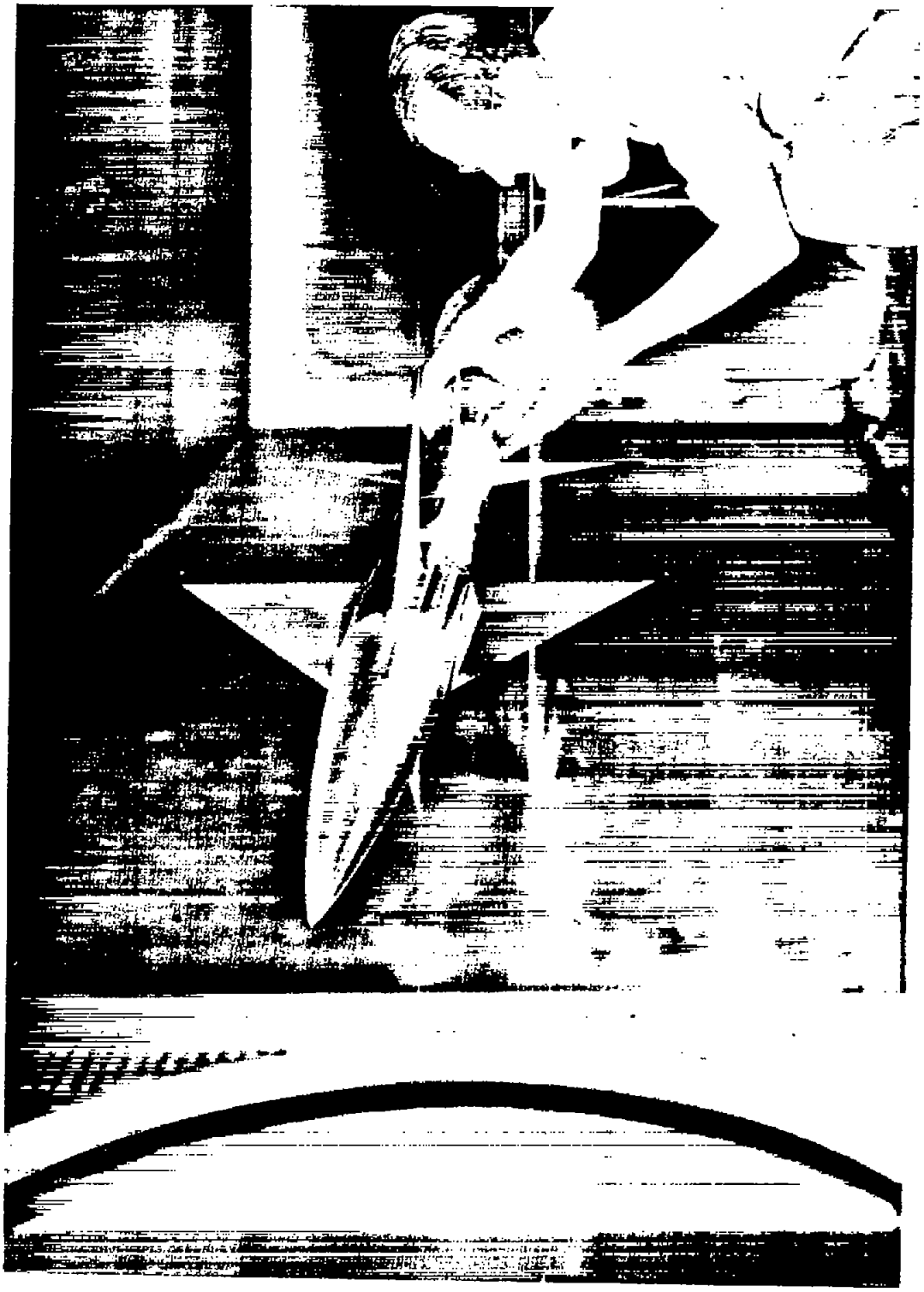

Figure 2.- Model installation.

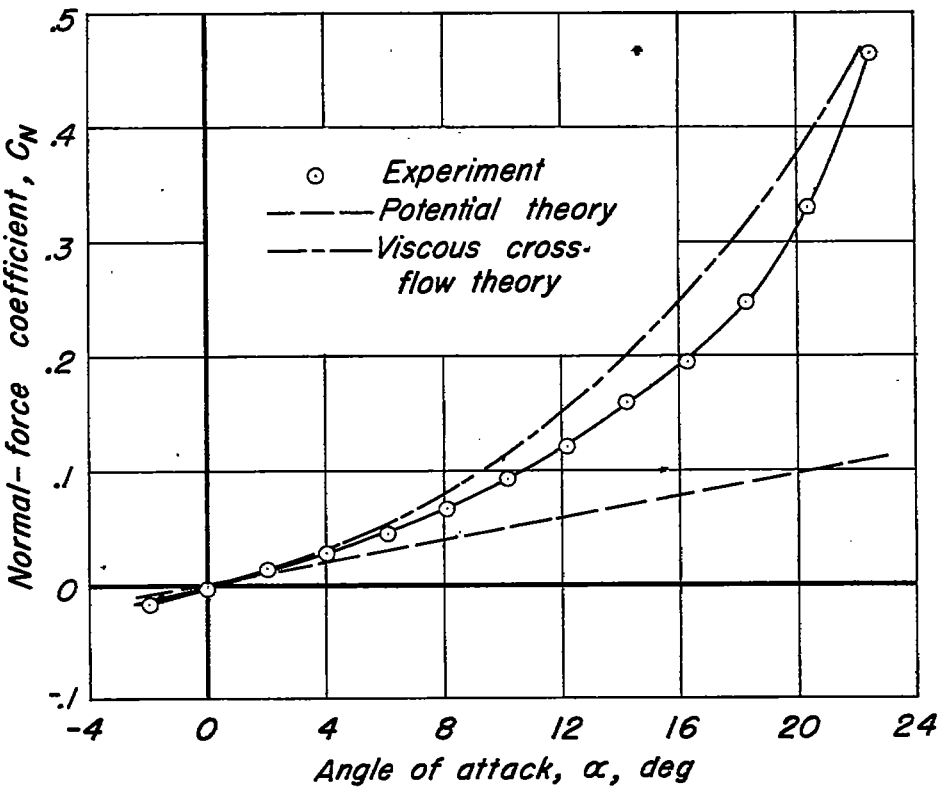

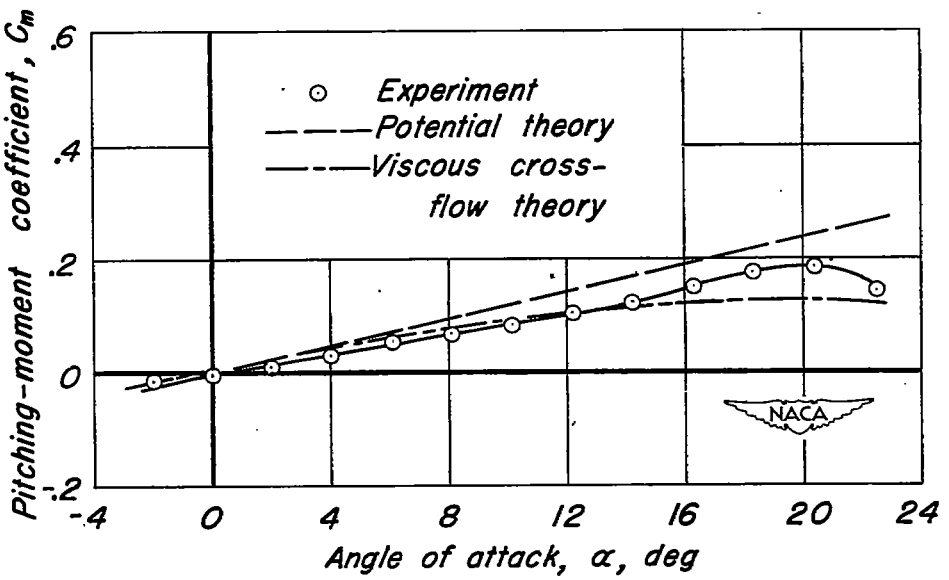

Figure 3.–Characteristics of body.

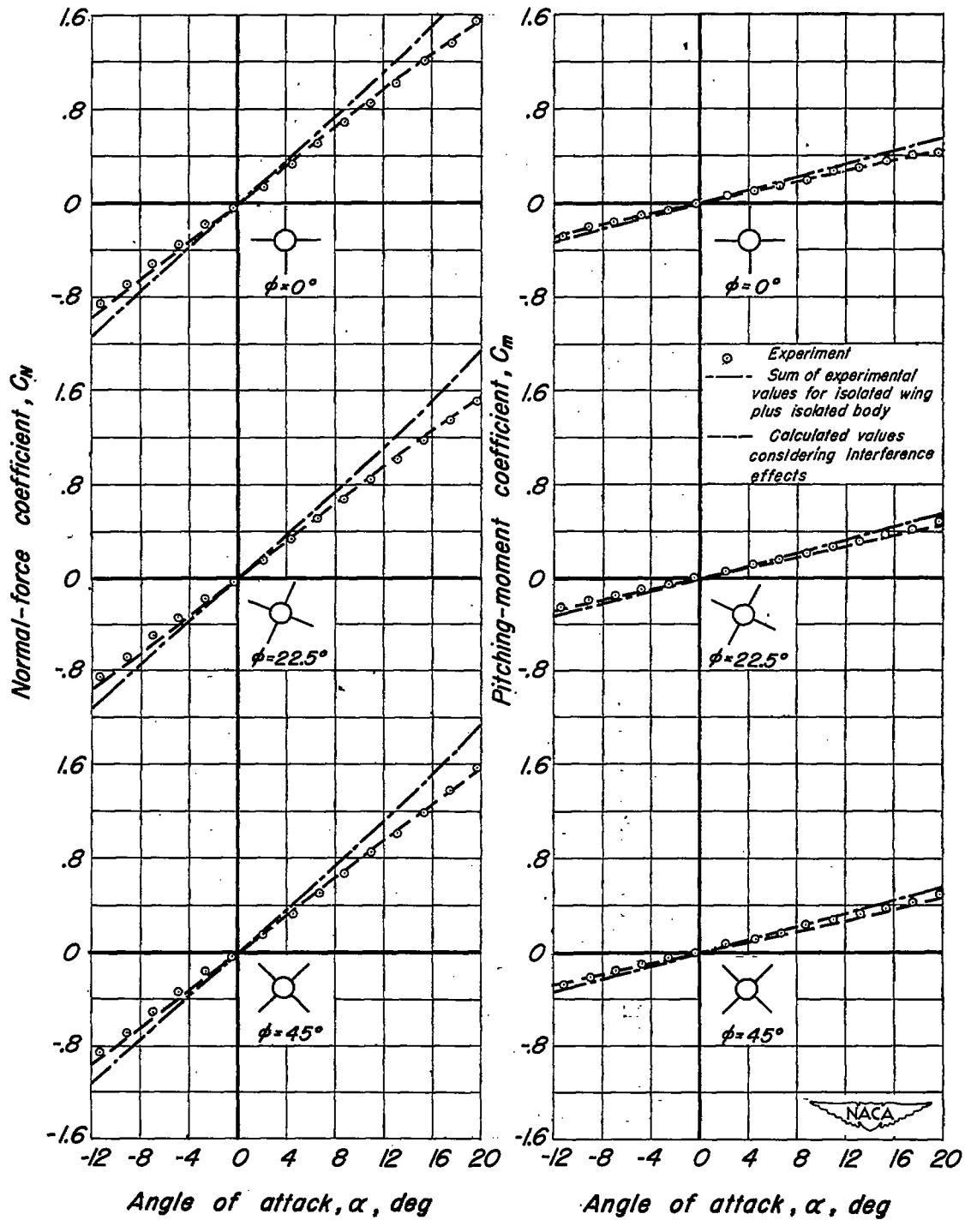

Figure 4.-Characteristics of wing plus body.

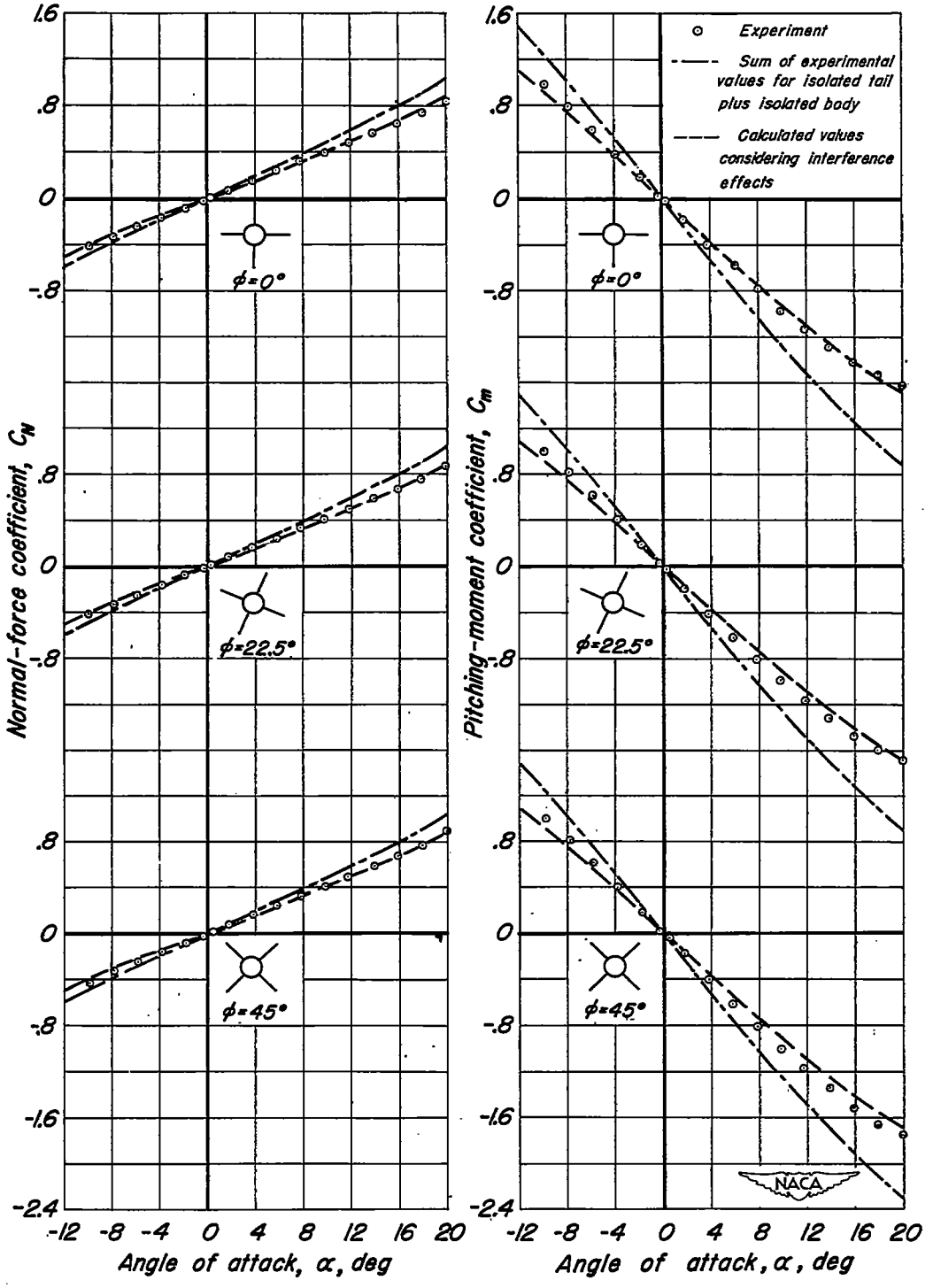

Figure 5.–Characteristics of tail plus body.

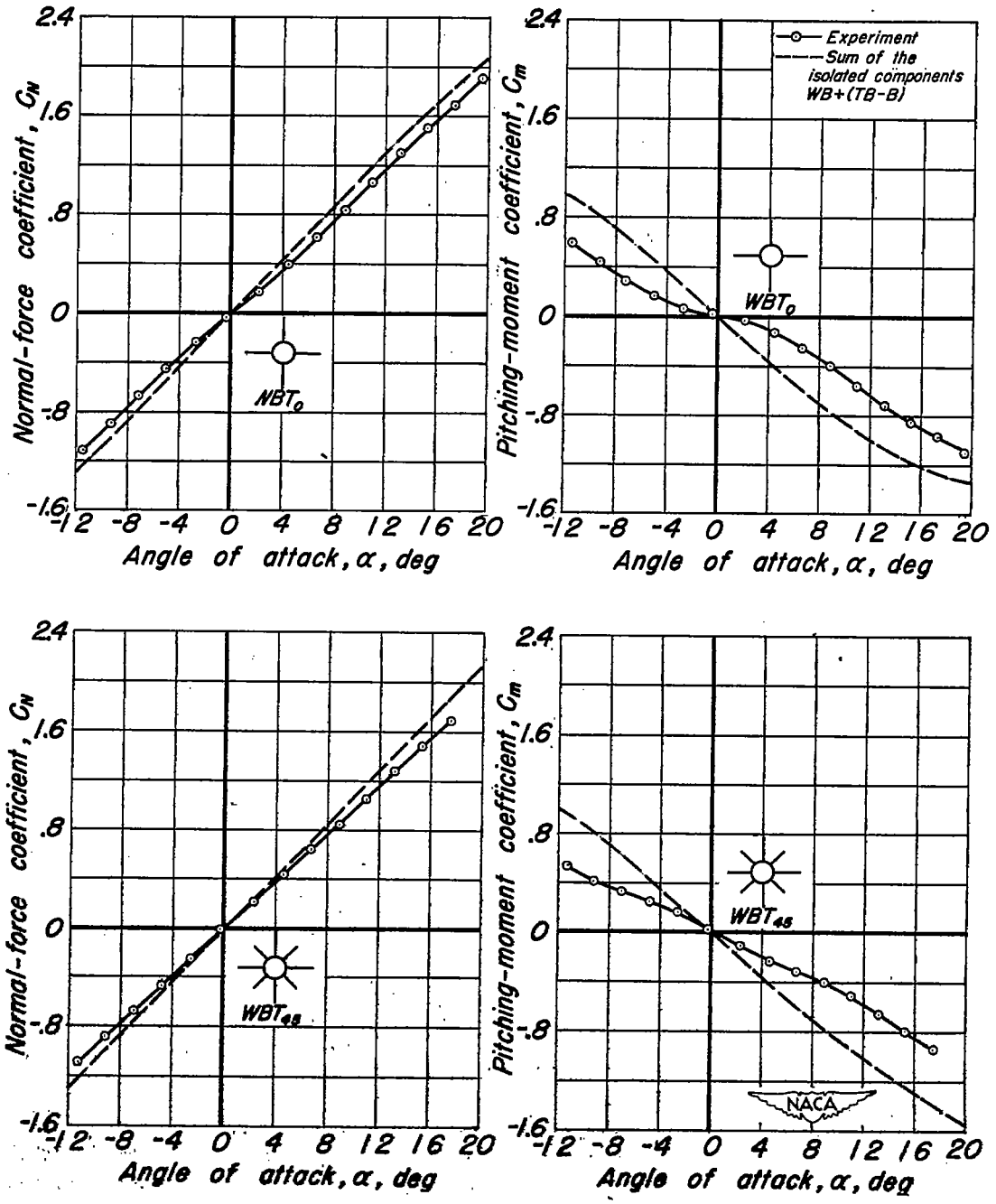

(a) $\phi = 0°$

Figure 6.-Characteristics of complete configurations.

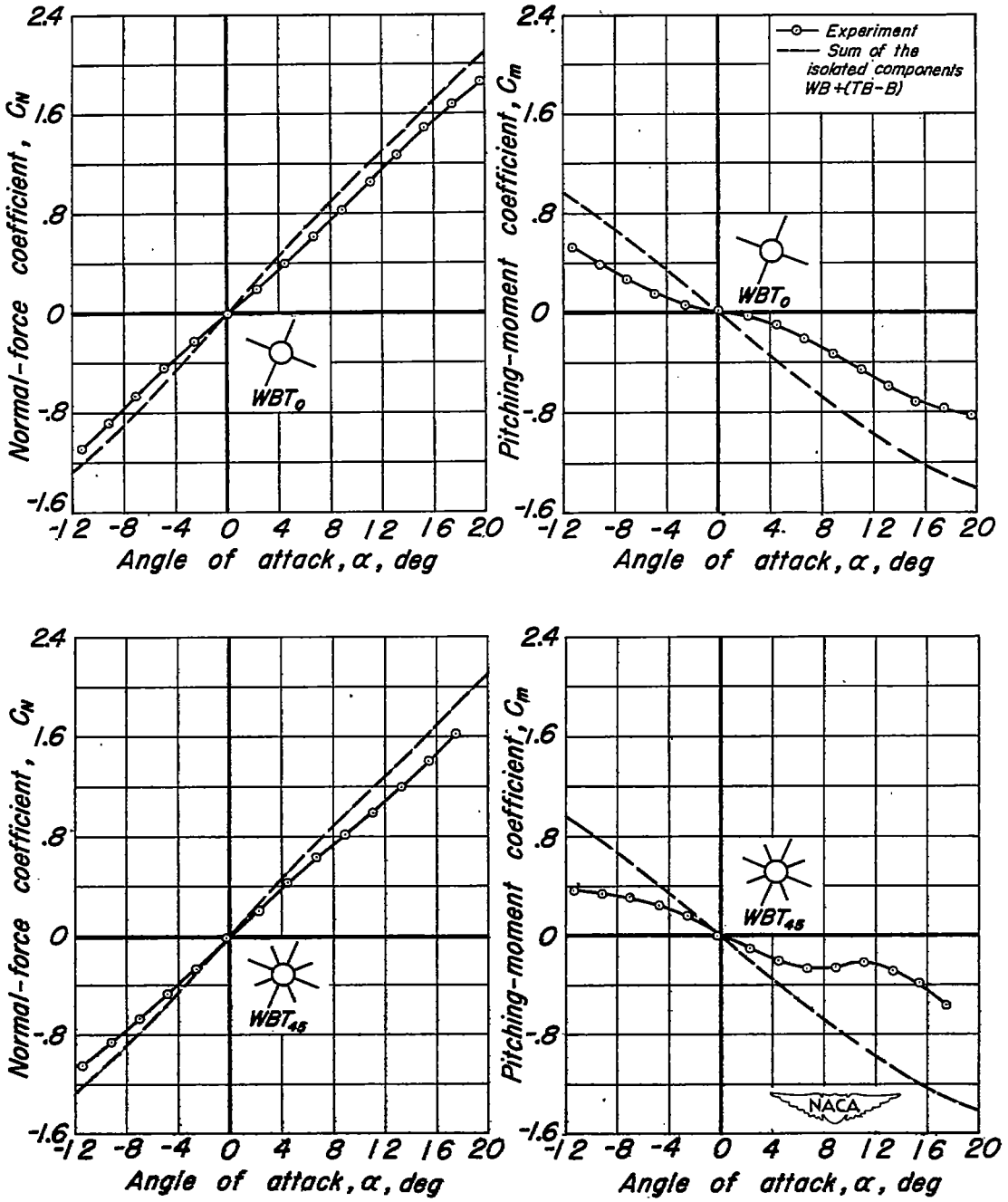

(b) $\phi = 22.5°$

Figure 6.-Continued.

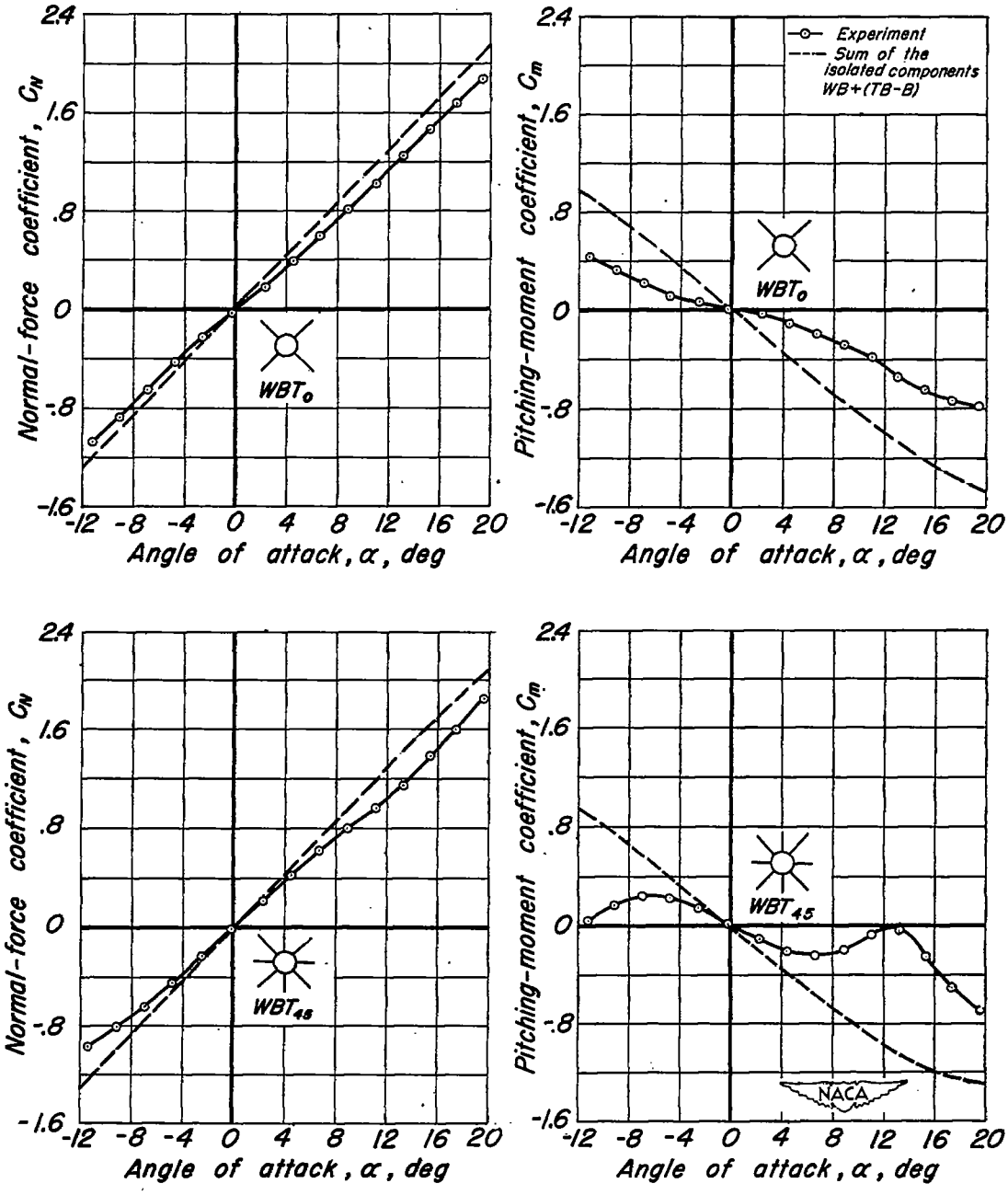

(c) $\phi = 45°$

Figure 6.-Concluded.

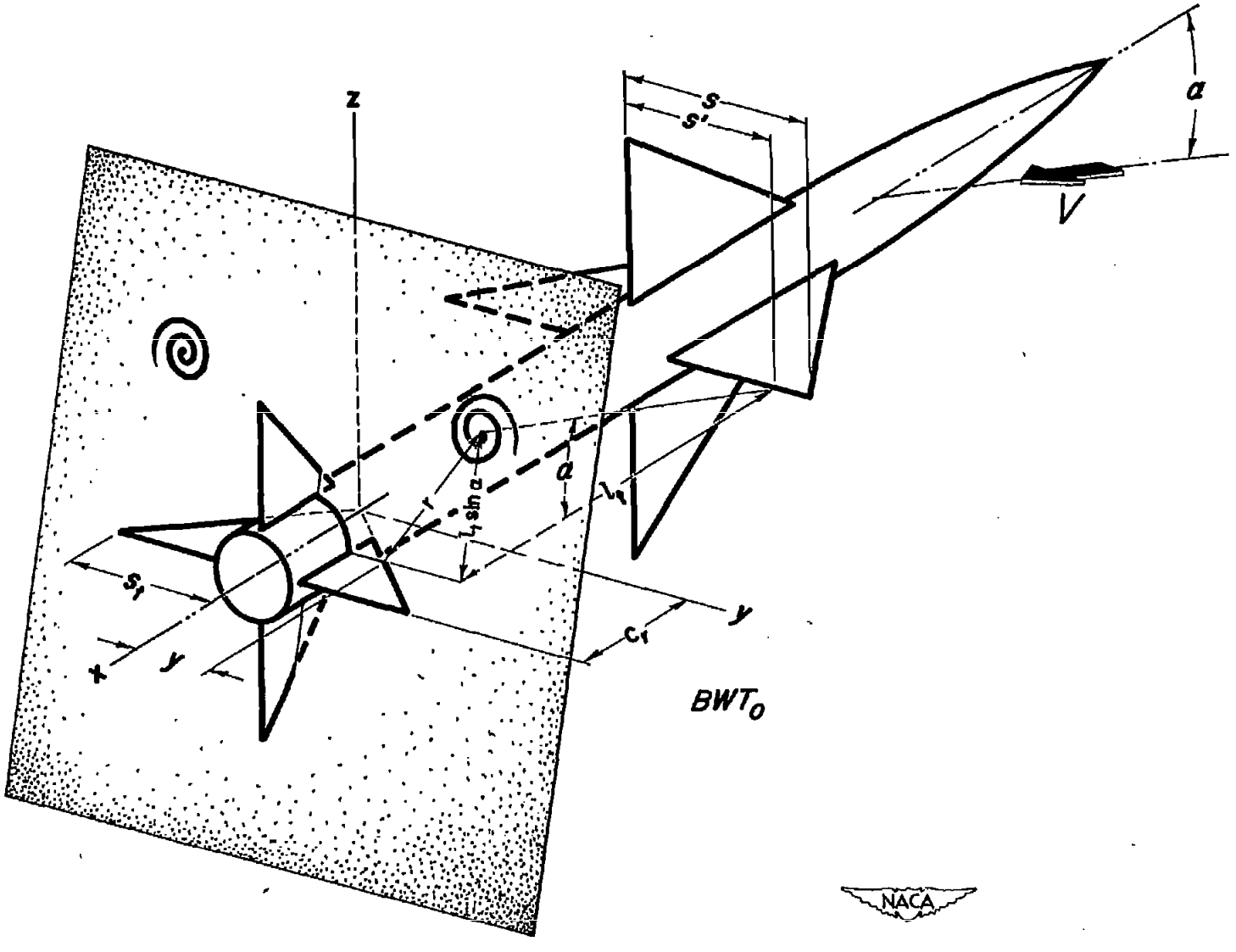

Figure 7.– Geometric relations for obtaining spanwise variation of downwash angle at tail due to completely rolled-up vortices behind wing trailing edge.

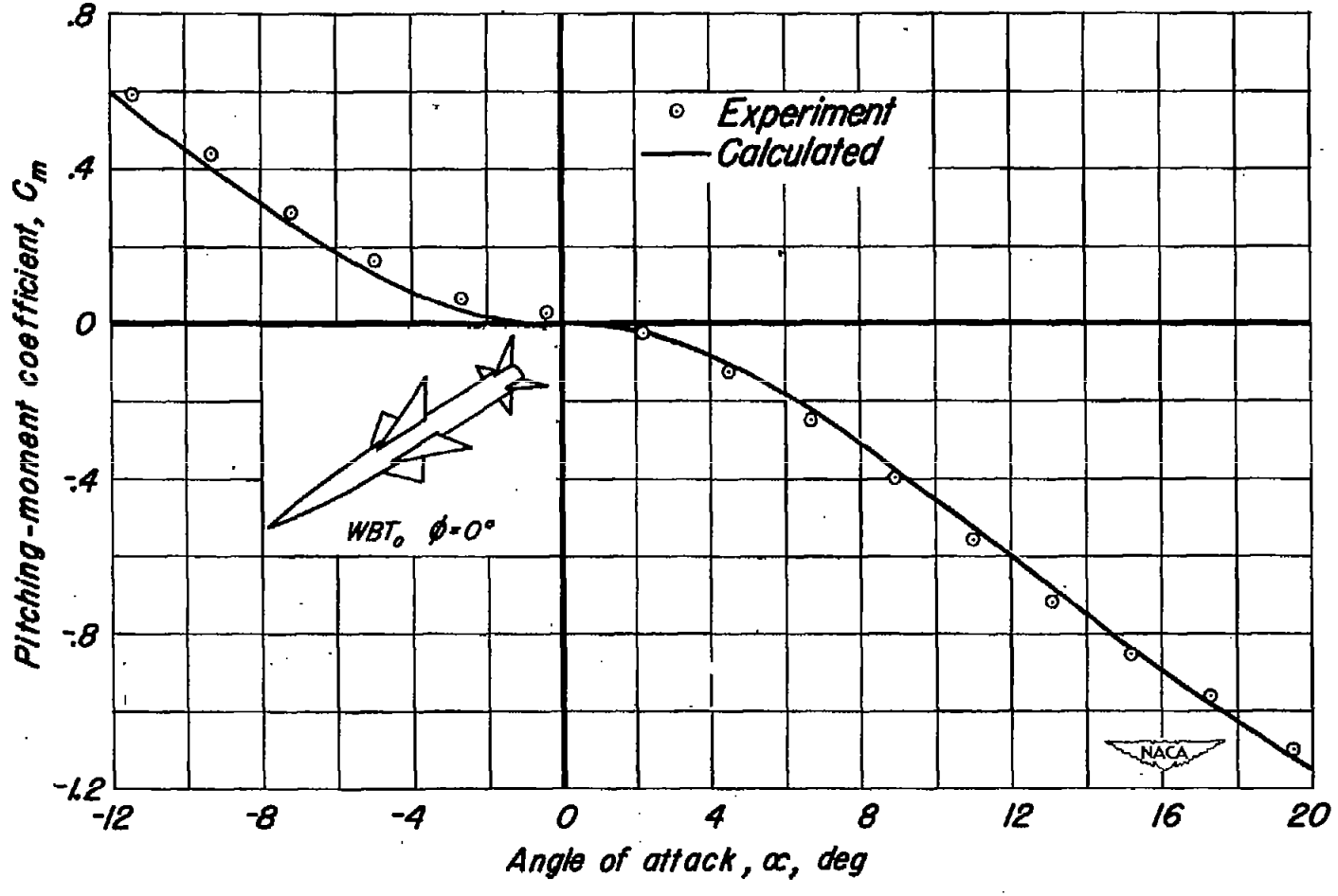

Figure 8.– Pitching-moment characteristics of the complete configuration with the tail in line obtained from experiment and from calculations assuming fully rolled-up vortices.

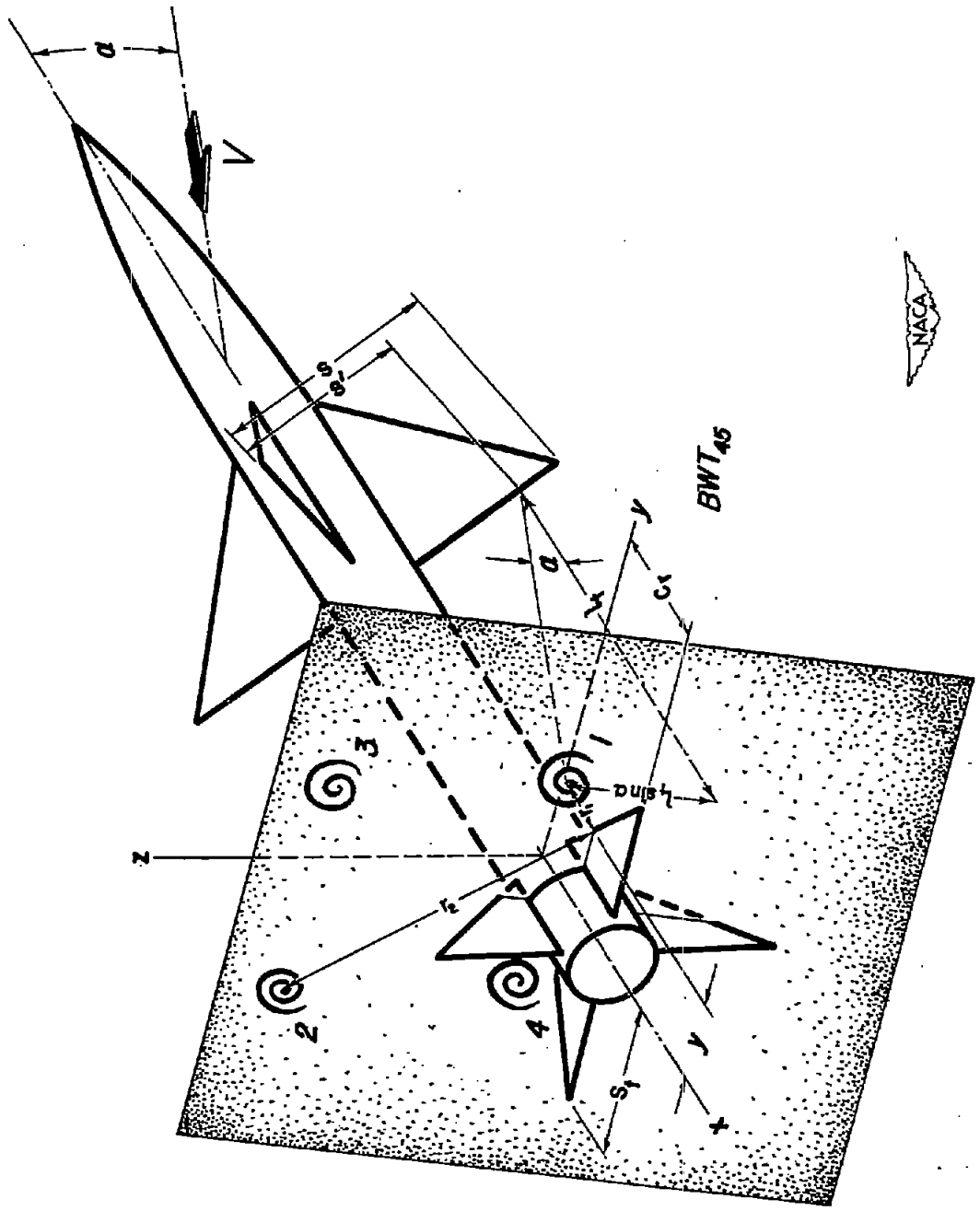

Figure 9.- Geometric relations for obtaining the spanwise variation of the downwash angle at the tail due to completely rolled-up vortices behind the cruciform wing banked at 45°.

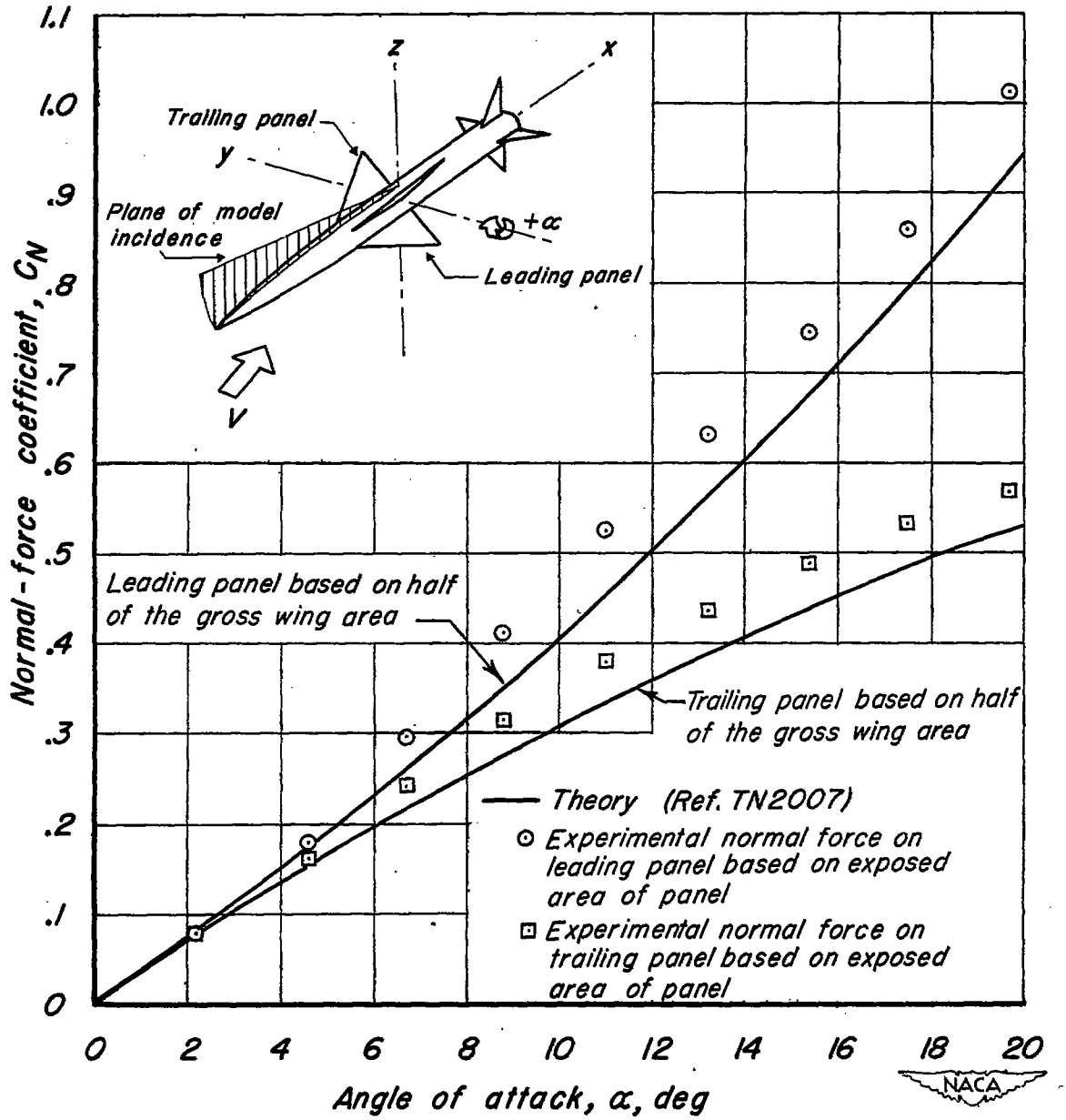

Figure 10.– Experimental and theoretical normal-force coefficients on the leading and trailing panels of a 60° triangular wing banked at 45°.

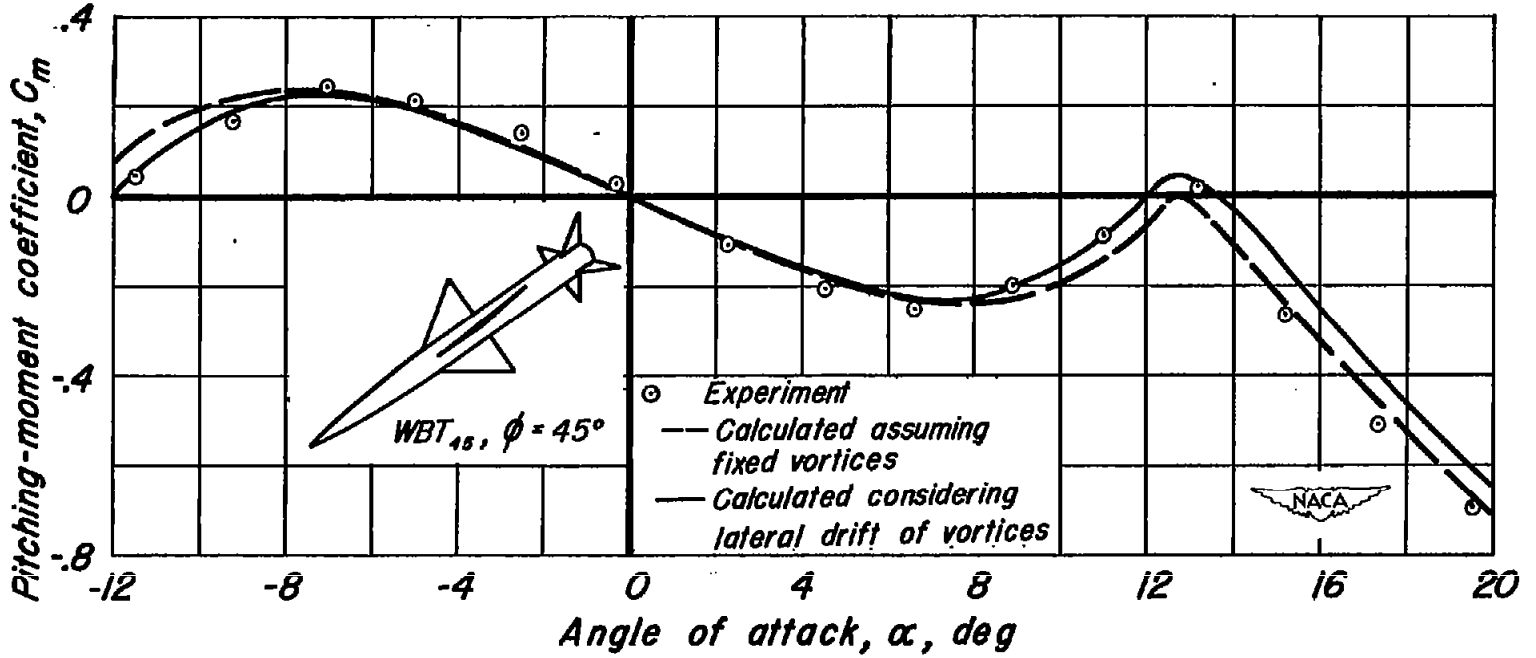

Figure 11.— Pitching-moment characteristics of the complete configuration with the tail interdigitated obtained from experiment and from calculations assuming fully rolled-up vortices.